HAL
open science

Granulosa cells provide elimination of apoptotic oocytes through unconventional autophagy-assisted phagocytosis

M.G. Yefimova, C Lefevre, Anu Bashamboo, C Eozenou, A Burel, M. T. Lavault, Ac Meunier, C Pimentel, S Veau, A. S. Neyroud, et al.

To cite this version:

M.G. Yefimova, C Lefevre, Anu Bashamboo, C Eozenou, A Burel, et al.. Granulosa cells provide elimination of apoptotic oocytes through unconventional autophagy-assisted phagocytosis. Human Reproduction, 2020, 35 (6), pp.1346-1362. 10.1093/humrep/deaa097 . hal-02888701

HAL Id: hal-02888701

https://hal.science/hal-02888701

Submitted on 10 Jul 2020

HAL is a multi-disciplinary open access archive for the deposit and dissemination of scientific research documents, whether they are published or not. The documents may come from teaching and research institutions in France or abroad, or from public or private research centers.

L'archive ouverte pluridisciplinaire **HAL**, est destinée au dépôt et à la diffusion de documents scientifiques de niveau recherche, publiés ou non, émanant des établissements d'enseignement et de recherche français ou étrangers, des laboratoires publics ou privés.

Granulosa cells provide elimination of apoptotic oocytes through unconventional autophagy-assisted phagocytosis

M.G. Yefimova[1,2*], C. Lefevre[3], A. Bashamboo[4], C. Eozenou[4], A. Burel[5], M.T. Lavault[5], A.C. Meunier[6], C. Pimentel[1], S. Veau[1], A.S. Neyroud[1], S. Jaillard[1], B. Jégou[3], N. Bourmeyster[6,7], C. Ravel[1,3].

[1]Département de gynécologie obstétrique et reproduction humaine - CECOS, CHU de Rennes, 16, boulevard de Bulgarie, 35000 Rennes, France

[2]Sechenov institute of evolutionary physiology and biochemistry, Russian academy of sciences, 44, M. Thorez pr., St-Petersburg 194223, Russia

[3]Univ Rennes, Inserm, EHESP, Irset (Institut de recherche en santé, environnement et travail) - UMR_S 1085, F-35000 Rennes, France

[4]Human Developmental Genetics, Institut Pasteur, 25-28 Rue du Docteur Roux, Paris 75724, France.

[5]MRic TEM Plateform, BIOSIT, Université Rennes 1, 2, avenue du Pr Léon-Bernard, 35000 Rennes, France.

[6]Laboratoire STIM, Université de Poitiers, 1, rue Georges-Bonnet, 86022 Poitiers cedex, France.

[7]CHU de Poitiers, 2 Rue de la Milétrie, 86021 Poitiers cedex, France

Corresponding author: Marina G. Yefimova*; E-mail: yefimova3@gmail.com

Running title: Granulosa cells ingest and destroy the apoptotic oocytes

Accepted manuscript

25 **Abstract**

26 **STUDY QUESTION**: Do human granulosa cells (GC) ingest and destroy apoptotic oocytes?

27 **SUMMARY ANSWER:** Somatic GC ingest and destroy apoptotic oocytes and other apoptotic
28 substrates through unconventional autophagy-assisted phagocytosis.

29 **WHAT IS KNOWN ALREADY:** Most (99%) ovarian germ cells undergo apoptosis through
30 follicular atresia. The mode of cleaning of atretic follicles from the ovary is unclear. Ovarian GC
31 share striking similarities with testicular Sertoli cells with respect to their origin and function.
32 Somatic Sertoli cells are responsible for the elimination of apoptotic spermatogenic cells through
33 unconventional autophagy-assisted phagocytosis.

34 **STUDY DESIGN, SIZE, DURATION:** Human GC were tested for the ability to ingest and
35 destroy the apoptotic oocytes and other apoptotic substrates. A systemic study of the main
36 phagocytosis steps has been performed at different time points after loading of apoptotic
37 substrates into the GC.

38 **PARTICIPANTS/MATERIALS, SETTING, METHODS:** Primary cultures of GC retrieved
39 following controlled ovarian stimulation of five women for IVF/ICSI and a human granulosa
40 KGN cell line were incubated with different apoptotic substrates: oocytes which underwent
41 spontaneous apoptosis during the cultivation of immature germ cells for IVF/ICSI; apoptotic
42 KGN cells; and apoptotic membranes from rat retinas. Cultured GC were analyzed for the
43 presence of specific molecular markers characteristic of different steps of phagocytic and
44 autophagy machineries by immunocytochemistry, confocal microscopy, transmission electron
45 microscopy and western blotting, before and after loading with apoptotic substrates.

46 **MAIN RESULTS AND THE ROLE OF CHANCE:** Incubation of human GC with apoptotic
47 substrates resulted in their translocation in cell cytoplasm, concomitant with activation of the
48 phagocytosis receptor c-mer proto-oncogene tyrosine kinase MERTK ($P<0.001$), clumping of

Accepted manuscript

motor molecule myosin II, recruitment of autophagy proteins: autophagy related protein 5 (ATG5), autophagy-related protein 6 (Beclin1) and the rise of a membrane form of microtubule-associated protein 1 light chain 3 (LC3-II) protein Ingestion of apoptotic substrates was accompanied by increased expression of the lysosomal protease Cathepsin D ($P<0.001$), and a rise of lysosomes in the granulosa cells, as assessed by different techniques. The level of autophagy adaptor, sequestosome 1/p62 (p62) protein remained unchanged.

LARGE SCALE DATA: N/A

LIMITATIONS, REASONS FOR CAUTION: The number of patients described here is limited. Also the dependence of phagocytosis on reproductive hormone status of patients should be analyzed.

WIDER IMPLICATIONS OF THE FINDINGS: Removal of apoptotic oocytes by surrounding GC seems likely to be a physiological mechanism involved in follicular atresia. Proper functioning of this mechanism may be a new strategy for the treatment of ovarian dysfunctions associated with an imbalance in content of germ cells in the ovaries, such as premature ovarian failure and polycystic ovary syndrome.

STUDY FUNDING/COMPETING INTEREST(S): The study was funded by Rennes Metropole (AIS 2015) and Agence de BioMédecine. This work was supported by funding from Université de Rennes1, Institut National de la Santé et de la Recherche Médicale (INSERM) and CHU de Rennes. A. Bashamboo is funded in part by the program Actions Concertées Interpasteuriennes (ACIP) and a research grant from the European Society of Pediatric Endocrinology. This work is supported by the Agence Nationale de la Recherche Grants ANR-17-CE14-0038 and ANR-10-LABX-73. The authors declare no competing interests.

TRIAL REGISTRATION NUMBER: GMR 2017-03

Accepted manuscript

Key words: granulosa cells/apoptotic oocytes/follicular atresia/phagocytosis/autophagy/LC3-associated phagocytosis/ Sertoli cells/photoreceptor outer segments/premature ovarian failure/polycystic ovary syndrome

Introduction

Apoptosis is a vital process that occurs in normal and pathological conditions in all tissues of the body (Elmore, 2007). Once formed, apoptotic cells are immediately eliminated by cells endowed with phagocytic activity. Phagocytosis of apoptotic cells or cell debris is a complex receptor-mediated process. The coordinated action of membrane-bound receptors triggers signaling mechanisms, which stimulate the ingestion of apoptotic substrates for their further degradation by lysosomal enzymes (Yefimova et al., 2018). Using specific receptors, phagocytes recognize and bind to the specific "eat-me" signals appearing on apoptotic cell surfaces, such as externalized phosphatidylserine (PS) (Wu et al., 2006). Both the timely and complete clearance of apoptotic substrates is important to maintain tissue homeostasis, and to avoid the autoimmune response against intracellular antigens (Itoh et al., 1999).

The mammalian ovary is an extremely dynamic organ, in which 99 % of ovarian germ cells undergo apoptosis through follicular atresia (Matsuda et al., 2012). Atresia can affect the follicles at all stages of their development, so that both oocytes and surrounding granulosa cells (GC) go through cell death. The pattern of atresia depends on the phase of follicular maturation. Thus, in primordial, primary and small pre-antral follicles apoptotic cell death affects oocytes, while in late pre-antral, antral and ovulatory follicles, apoptosis triggers granulosa cell death (reviewed by Yadav et al., 2018). The mode of removal of the atretic follicles from the ovary remains unknown (Yadav et al., 2018). Indeed, the blood-follicular barrier protects ovarian tissue from blood-circulating phagocytes (Siu & Cheng, 2012). Besides, resident ovarian macrophages exhibit a very limited ability to phagocytose the extrinsic substrates (Itoh et al., 1999). The role

Accepted manuscript

of these immune cells is mainly related to folliculogenesis regulation, but not to phagocytic function (Katabushi et al, 1996; Gaytánet al., 1998; Wu et al., 2004; Ono et al., 2018).

Massive cell death also occurs in the male reproductive system, wherein 75% of spermatogenic cells undergo apoptosis in blood-separated seminiferous tubules (Shaha et al., 2010). Removal of apoptotic substrates is carried out by the somatic Sertoli cells (Jégou, 1993; Yefimova et al., 2018), which share striking similarities with ovarian GC with respect to their origin and function (Mork et al., 2012). Phagocytic elimination of apoptotic substrates by the Sertoli cells proceeds through LC3-associated phagocytosis (LAP), a hybrid process in which the phagocytic machinery is supported by autophagy degradation (Sanjuan et al., 2007; Yefimova et al., 2013; Panneerdoss et al., 2017).

In contrast to phagocytosis, which provides the degradation of extracellular substrates, autophagy is a lysosome-dependent degradation pathway, which destroys the different substrates of intracellular origin (Mizushima et al., 2008; Yin et al., 2016). Autophagy can be initiated by different stimuli, including nutrient deprivation, metabolic and infection-mediated stresses, cancer, neurodegeneration, and others. Autophagy is regulated by the autophagy-related (*ATG*) genes, which were originally identified in yeast, and their mammalian homologs (Mizushima et al., 2011). Before degradation within the lysosome, substrates to be eliminated are enclosed in an autophagosome, which is a double membrane-limited vacuole containing a lipidated form of LC3 protein (ATG8): the latter is currently used as a molecular marker to monitor autophagy (Klionsky et al., 2016).

Exploitation the autophagy component by phagocytosis machinery increases its efficiency, providing rapid lysosomal fusion and cargo degradation (Heckmann et al., 2017). The term LAPosome was proposed to define the particular structure, which harbors the substrate for degradation by LAP. In contrast to an autophagic vacuole, the LAPosome is a single-membrane vesicle coated with lipidated LC3 protein. The presence of LC3 protein distinguishes a LAPosome from the single-membrane phagosome vesicle (Heckmann et al., 2017). LAP-specific

Accepted manuscript

genes include *ATG5,* autophagy-relared gene 7 *(ATG7), Beclin1, Rubicon* (RUN domain and cysteine-rich domain containing Beclin 1-interacting protein) *and NOX2* (NADPH oxidase-2) (Bandyopadhyay & Overholtzer, 2016). While using several autophagy proteins, LAP is independent of the autophagy preinitiation complex (ATG13-ULK1 (Unc-51 like autophagy activating kinase 1)-RB1CC1/FIP200 (RB1 inducible coiled-coil 1)-ATG101) (Kim et al., 2013; Martinez et al., 2015; Masud et al., 2019). In macrophages and in retinal pigmented epithelial cells, autophagy components ATG5, ATG7, ATG3, ATG12 , ATG16L1 and a Beclin1-PIK3C3 (Phosphatidylinositol 3-Kinase Catalytic Subunit Type 3)/VPS34 (vacuolar protein sorting) complex lacking ATG14 are engaged in the lipidation of LC3 protein and its recruitment to the phagosome. LAP also requires Rubicon for proper function (Martinez et al., 2015; Muniz-Feliciano et al., 2017). Beclin1, ATG5 and Rubicon proteins have been detected in LAPosomes from different types of phagocytic cells (blood macrophages, retinal pigmented epithelial cells) that use LAP (Amer & Swanson, 2005; Martinez et al., 2011; Wirawan et al., 2012; Kim et al., 2013; Martinez et al., 2015).

The phagocytic ability of GC *in situ* has been noticed by numerous investigators, who observed ingested material in the cytoplasm of GC at all stages of follicular development (cited from Kasuya, 1997; Gaytan et al., 1998). Living GC eliminate their apoptotic counterparts produced during follicular atresia (Kasuya, 1997; Gaytán et al., 1998). GC from atretic follicles show an activation of autophagy (Yadav et al., 2018) and increased expression of the phagocytosis receptor MERTK (Hatzirodos et al., 2014), which is the main receptor mediating the ingestion of apoptotic substrates during LAP (Kim et al., 2013; Yefimova et al., 2013; Panneerdoss et al., 2017). These data suggest the involvement of both phagocytosis and the autophagy degradation machinery in the process of follicular atresia.

Paradoxically, a possible involvement of GC in the elimination of apoptotic germ cells/oocytes has never been considered. In this work, we aimed to test the ability of GC to ingest and destroy the apoptotic oocytes as well as other apoptotic substrates, and to get insights into

Accepted manuscript

149 molecular mechanisms of this process. Using the human granulosa cell line KGN and primary
150 cultures of human GC, we undertook a systemic study of the main steps involved in the ingestion
151 and degradation of apoptotic substrates, using cytochemistry, immunocytochemistry, electron
152 microscopy and western blotting (WB). In our *in vitro* study we show for the first time that GC
153 efficiently phagocytose apoptotic oocytes as well as other apoptotic substrates. Intracellular
154 management of ingested substrates is facilitated by autophagy degradation machinery through a
155 process strongly resembling LAP, which is responsible for the degradation of apoptotic germ
156 cells by the somatic Sertoli cells from the testis.

157

158 **Materials and Methods**

159 Cells, cell cultures and animals

160 *Primary culture of human GC*

161 GC samples were provided by the BioBankGermetheque (BBMRI, France). Fresh GC
162 were retrieved following controlled ovarian stimulation for IVF/ICSI from five patients
163 submitted to standard protocols (Jungheimet al., 2015). All patients signed an informed consent.
164 GCs were isolated from corona radiata and a part of the cumulus oophorus. This suspension was
165 enzymatically treated using 80 IU Hyaluronidase (HYA001; FertiPro NV, Belguim) to separate
166 oocytes from GCs. Oocytes were evacuated with a glass capillary and afterwards, inactivation
167 medium was added into the GCs suspension. GCs inactivation medium consisted of M199
168 medium (M3769; Sigma, St. Louis, MO, USA), supplemented with 20% fetal calf serum (FCS,
169 12133C; Sigma, St. Louis, MO, USA) and 1% antibiotic mix (10 000 U/ml penicillin and 50
170 mg/ml streptomycin, 15140; Gibco Waltham, MA, USA). GCs suspension was centrifuged at
171 450g for 10 min at 20°C, and then the pelleted cells were suspended in supplemented M199
172 medium (see above) and seeded in the 5-well culture dish for denudation (16004; Vitrolife,
173 Sweden).

174

Accepted manuscript

175 *Human apoptotic oocytes*

176 During the cultivation of immature oocytes, some of them undergo a spontaneous
177 apoptosis (Wu et al., 2000). Oocytes exhibiting morphologic features of apoptosis, such as
178 shrinkage, cytoplasmic condensation, membrane blebbing, and/or nuclear fragmentation (Kerr et
179 al., 1972), were collected and stored at – 195°C before being used as a substrate for phagocytosis
180 studies.

181

182 Human granulosa KGN cells were from Pasteur's Institute (Paris, France); human
183 telomerase-immortalized retinal pigment epithelium hTERT-RPE1 cells were from Clonetech
184 (C4000-1; Mountain View, CA, USA). KGN GC were cultured in DMEM/F12 medium (31331;
185 Gibco, Waltham, MA, USA), containing 10% FCS (12133C; Sigma, St. Louis, MO, USA) and
186 supplemented with 1% antibiotic mix (15140; Gibco, Waltham, MA, USA). hTERT-RPE1 cells
187 were cultured in DMEM/F12 medium (31330; Gibco, Waltham, MA, USA), supplemented with
188 10% FCS (12133C; Sigma, St. Louis, MO, USA) and 1% antibiotic mix (as above). For
189 immunocytochemistry experiments 1.5×10^5 of KGN or RPE-1 cells were seeded in 8-well
190 Labtek chamber slides (177402; Thermofisher, Waltham, MA, USA) pre-coated with the
191 Fibronectin (F1141; Sigma, St. Louis, MO, USA) according to the manufacturer's protocol. For
192 WB, experiments $5x10^5$ cells were plated into 6-well dishes and cultured at 37°C with 5% CO_2.
193 All cell lines were tested for mycoplasma contamination using mycoplasma detection kit
194 (MycoAlert LT07; LONZA, Basel, Switzerland).

195 Male Wistar rats, aged 2 months, were obtained from Janvier Labs (RjHan: WI; France).

196

197 Pharmacological reagents and antibodies

198 Dulbecco's PBS (D5652), bovine serum albumin (BSA) (A9647), ceramide (22244),
199 lead(II) nitrate (228621), ammonium sulfide solution (A1952), rapamycin (R8781), β-
200 glycerophosphate (G-9422), fluorescein isothiocyanate (FITC) (F7250) and 1 μm diameter

Accepted manuscript

201 carboxylate-modified polystyrene fluorescent beads (L4530) were from Sigma-Aldrich (St.
202 Louis, MO, USA). Polyclonal rabbit primary antibodies anti-ATG5 (NB110-53818), anti-
203 Beclin1 (NB500-249), anti-LC3B (NB100-2220), anti-p62/SQSTM1 (NBP1-48320), anti-zona
204 pellucida glycoprotein 3 (ZP3) (NBP2-30830) and anti-phospho-MERTK (NB300-690) from
205 Novus Biologicals Centennial, CO, USA, and polyclonal goat primary antibody anti–Cathepsin
206 D (sc-6486) was from Santa-Cruz Biotechnology, Santa Cruz, CA, USA. The monoclonal mouse
207 antibodies used were anti-rhodopsin (1D4) (sc-57432; Santa-Cruz Biotechnology, Santa
208 Cruz, CA, USA,) anti-myosin heavy chain antibody (3-48) (NB300-284; Novus Biologicals
209 Centennial, CO, USA), anti-ATG7 (sc-376212; Santa-Cruz Biotechnology, Santa Cruz, CA
210 USA) and anti-GAPDH (sc-47724; Santa-Cruz Biotechnology, Santa Cruz, CA USA). The other
211 antibodies conjugated to horse-radish peroxidase were: secondary anti-rabbit (NA934; GE
212 Healthcare, Chicago, IL, USA), anti-mouse (NA931; GE Healthcare, Chicago, IL, USA) and
213 anti-goat (sc-2020; Santa Cruz Biotechnology, Santa Cruz, CA, USA); for immunostaining: anti-
214 rabbit, anti-mouse, and anti-goat antibodies conjugated to Alexa-488 (CAR-A21441), to Alexa-
215 555 (GAM-A21422, DAM-A31570) from Molecular Probes (Invitrogen; Carlsbad, CA, USA) or
216 to FP-647 (GAR-FPGARBTTG0642) from Interchim (Montflucon, France).
217

218 Isolation of photoreceptor outer segments

219 Photoreceptor outer segments (POS) have externalized PS on their outer membrane
220 leaflet, therefore are currently used as apoptotic-like substrate for phagocytosis studies
221 (Finnemann et al., 1997; Yefimova et al., 2013).

222 POS were isolated from the eyes of 2-month-old Wistar rats as described earlier
223 (Yefimova et al., 2013). Briefly, the rats were euthanized with CO_2. Freshly enucleated eyes
224 were dissected, the retinae were removed from the eyecups and suspended in 0.3M
225 Mannitol/PBS solution, pH 7.4 (0°C), containing 1% antibiotic mix (10 000 U/ml penicillin and
226 50 mg/ml streptomycin, 15140; Gibco, Waltham, MA, USA), and then vortexed for 20-60 sec

Accepted manuscript

227 and allowed to stand until the retinae settled. The supernatant containing the POS was collected,
228 centrifuged at 10 000 g for 15 min. To eliminate the traces of mannitol, the pellet containing
229 POS was washed twice with PBS medium supplemented with antibiotic mix (see above). Before
230 the second centrifugation, the suspension of POS was aliquoted in 1.5 ml Eppendorf tubes and
231 centrifuged again. After removing the supernatant, the aliquoted POS were stored in "dry" form
232 at -80°C before use. Each tube contained the POS from one retina.
233
234 Ceramide treatment
235 To induce apoptosis, cultured KGN cells were exposed to 10 µm exogenous ceramide for
236 24h (Davis et al., 2000). The next day the cells were scraped from 6-well dishes, counted, and
237 used as a phagocytosis substrate.
238
239 FITC labeling for immunofluorescence analysis
240 For immunofluorescence (IF) analysis, phagocytosis substrates (apoptotic oocytes,
241 apoptotic KGN cells, POS) were labeled using 1mg/ml FITC in 0.1M Na-bicarbonate (pH 9.0)
242 for 1h at 4°C in the dark, then washed and suspended in PBS.
243
244 Phagocytosis experiments
245 24h after the seeding of primary human GC, KGN and hTERT-RPE1 cells, the culture
246 media was replaced. The fresh culture media was the same, except that the content of FCS was
247 reduced to 2% in order to slow cell growth during experiments, and to minimize the modulatory
248 effect of serum on phagocytosis rate (Johnston et al., 1969). All phagocytosis substrates as POS,
249 apoptotic oocytes, apoptotic granulosa cells (labeled or unlabeled with FITC) or carboxylate-
250 modified polystyrene fluorescent beads (used as a control) were added to cells at a ratio 10/1.
251 The time of incubation of cells with phagocytosis substrates ranged from 0 to 24 hrs. At the end

Accepted manuscript

252 of the incubation, the cells were washed from unbound substrates with ice-cold PBS, and then
253 processed for immunocytochemistry or WB experiments.
254
255 Phagocytosis assay in rapamycin-treated cells
256 The KGN cells cultured in 8-well Labteck slides (see above) were incubated with 200 nM
257 rapamycin for 24 h, and the culture media was then replaced (as above) and the cells were
258 challenged with POS. At different time points from 0 to 2h, the cells were washed with ice-cold
259 PBS, fixed with 4% paraformaldehyde/PBS (pH 7.4), and then processed for the phagocytosis
260 test, allowing discrimination between bound and ingested substrates (Yefimova et al., 2008;
261 Yefimova et al., 2018). Briefly, the samples were divided into two groups, each in duplicate
262 wells. Group 1 was permeabilized with 0.5% Triton X-100 for 1 min, and group 2 remained
263 unpermeabilized. Then the cells were processed through immunofluorescence using anti-
264 rhodopsin antibody, as described below. The amount of total POS (plasma membrane bound and
265 ingested) was obtained from group 1, and the amount of plasma membrane-bound POS was
266 obtained from group 2. The amount of ingested POS was obtained by subtracting plasma
267 membrane bound POS from total POS. The phagocytosis index was calculated as the ratio of
268 POS area/nuclei area using Image J software (NIH, Bethesda, MD, USA).
269
270 Western blotting
271 Proteins were isolated from cell extracts obtained after lysis of 10^7 KGN or hTERT-RPE1
272 cells growing in 6-well dishes. Cells were washed with cold PBS, then collected by scraping on
273 ice in lysis buffer (50 µl/per well) containing 50 mM Tris-HCl, 150 mM NaCl, 1 mM EDTA, 1%
274 Triton X-100, phosphatase inhibitor cocktail (04906845001; Roche, Basel, Switzerland) and
275 protease inhibitor cocktail (11697498001; Roche, Basel, Switzerland). Then 4X Laemmli sample
276 buffer was added, and the samples were incubated at 99°C for 10 min. Proteins were separated
277 by electrophoresis on 12% sodium dodecyl-sulphate (SDS)-polyacrylamide gels, then transferred

Accepted manuscript

278 (2 h, 150 V) to nitrocellulose membranes (0.2 µm pore) (GE10600001; Amersham,
279 Buckinghamshire, UK). Blots were blocked for 2 h in TBS containing 5% (w/v) non-fat dry
280 milk. Blots were incubated with anti-phospho-MERTK (1/1000), anti-Beclin1 (1/1000), anti-
281 ATG5 (1/1000), anti-ATG-7 (1/500), anti-LC3 (1/1000), anti-Cathepsin D (1/1000) or anti-
282 GAPDH (1/1000) antibodies in TBS containing 0.5% (w/v) non-fat dry milk at 4°C overnight.
283 Membranes were then incubated with peroxidase-conjugated anti-rabbit (1/10000), anti-mouse
284 (1/10000) or anti-goat (1/5000) antibody in blocking buffer for 1 h at room temperature.
285 Immunodetection was performed with the chemiluminescence substrate Luminata
286 (WBLUF0500; Millipore, Burlington, MA, USA). In some cases, the blots were stripped in 25
287 mM Glycine-HCl buffer, containing 1% w/v SDS, pH 2 for 30 min; membranes were then
288 washed with TBS, blocked and re-probed as above. Densitometry analysis of specific bands on
289 the blots was performed using ImageJ (NIH, Bethesda, MD, USA) software. In phagocytosis
290 kinetic experiments the blots were normalized to time 0 (cells + phagocytosis substrate at the
291 time 0) to avoid the misinterpretation of the data due to the activation of degradation processes
292 during phagocytosis (see below).
293
294 Immunocytochemistry
295 Indirect immunofluorescence was performed following conventional procedures. Briefly,
296 cells growing on 8-well glass Labteck chamber slides were fixed in paraformaldehyde/PBS (pH
297 7.4), permeabilized with 0.5% Triton X-100/PBS, and then incubated overnight at 4°C with
298 primary antibodies diluted at a ratio 1:250 in 1% BSA/PBS. The dilution of the secondary
299 antibodies was 1:500 in 1% BSA/PBS. Cell nuclei were stained with DAPI (4', 6 diamidino-2-
300 phenylindole; 0.5 µg/ml) (62247, Thermo Fisher Scientific, Waltham, MA, USA). Slides were
301 observed under an inverted microscope: DMT 6000 Leica (Leica Microsystems; Wetzlar,
302 Germany). The pictures were taken using a DFC350FX camera (Leica Microsystems; Wetzlar,
303 Germany).

Accepted manuscript

304

305 Cytochemical analysis for lysosomes

306 In cytochemical experiments a modified Gomori protocol for lysosomal enzyme acid
307 phosphatase was used to stain the lysosomes in the GC (Allison & Mallucci, 1965). Gomori
308 reagent was prepared as follows: 660 mg of lead nitrate was dissolved in 50 ml of 2% solution of
309 β-glycerophosphate in 0.05M sodium-acetate buffer pH 5.0. The mixture was immediately
310 filtered through Whatman Filter paper.

311 KGN cells cultured on the 1-well glass Labteck slides were challenged with apoptotic
312 substrates. After incubation, the cells were washed in ice-cold PBS and fixed by immersion in -
313 20°C acetone for 40 min. Then the slides were air-dried and incubated in Gomori reagent at 37°
314 C for 6 h. After that the samples were washed in distilled water and immersed in ammonium
315 sulfide solution for 1 min. After washing in distilled water the slides were air-dried and analyzed
316 in Nanozoomer 2.0RS (Hamamatsu, Shizuoka, Japan) using NDP.view2 U12388-21 software
317 (version 2.7, Hamamatsu, Photonics, Japan). In each sample, the brown-stained area
318 corresponding to acid phosphatase was assessed by Image J software and assessed relative to the
319 number of nuclei in the sample.

320

321 Confocal microscopy

322 Samples were examined by confocal laser scanning microscopy using a confocal FV-
323 1000 station installed on an inverted microscope IX-81 (Olympus, France). Multiple
324 fluorescence signals were acquired sequentially to avoid crosstalk between image channels.
325 Fluorophores were excited with a 405 nm diode (for DAPI), 488 nm line of an argon laser (for
326 AF488), 543 nm line of a He-Ne laser (for AF555), and 633 nm line of a He-Ne laser (for AF647
327 and FP647). The emitted fluorescence was detected through spectral detection channels in the
328 range 425–475 nm, 500–530 nm, 555–655 nm and >680 nm for blue, green, red and far red
329 fluorescence, respectively. Maximal resolution was obtained with an Olympus UplanSapox60

Accepted manuscript

330 oil, 1.4 NA, objective lens (Olympus). When necessary, optical sectioning of the specimen (Z
331 series) was driven by a Z-axis stepping motor through the entire thickness of the cell layer.
332 Analysis of confocal images, co-localization studies evaluated with Pearson's correlation
333 coefficient, and modeling of 3D reconstruction images were performed with Imaris 3D (7.2.1)
334 software (Bitplane; Zurich, Switzerland).
335
336 Transmission electron microscopy
337 For transmission electron microscopy (TEM), KGN cells were fixed in 2.5%
338 glutaraldehyde (16220; Electron Microscopy Sciences, Hatfield, PA, USA)/0.1M cacodylate
339 buffer, pH 7.2 (11650; Electron Microscopy Sciences, Hatfield, PA, USA), at room temperature
340 for 1 h, then washed in cacodylate buffer for a further 30 min. The samples were postfixed in 1%
341 osmium tetroxide (19150; Electron Microscopy Sciences, Hatfield, PA, USA) for 1 h at room
342 temperature, then dehydrated through graded alcohol series (VWR Chemicals, 20821.296), and
343 embedded in Epon 812 medium (45345; Sigma Aldrich,St. Louis, MO, USA). Ultrathin sections
344 of 80 nm were cut using a Leica Ultracut UCT Ultramicrotome (Leica-Reichert; Leica
345 Microsystems; Wetzlar, Germany), contrasted with uranyl acetate and examined at 120 kV with
346 a JSM-4000 (JEOL; Tokyo, Japan) electron microscope. Images were captured digitally by an
347 Orius 1000 (Gatan, Abingdon, UK) camera.
348
349 Statistical analysis
350 The count of lysosomes was performed in TEM grids containing the cross-sections of
351 KGN cells loaded with apoptotic oocytes (24 cross-sections), POS (12 cross-sections) and
352 unloaded control KGN cells (8 cross-sections). Graph Pad Prism Software (San Diego, CA,
353 USA) was used to conduct statistical analysis using one-way ANOVA followed by Bonferroni
354 posthoc test. Differences were considered statistically significant for a value of $P < 0.05$ and $P<$
355 0.001.

Accepted manuscript

356

357 Ethical approval

358 Human samples were provided by GERMETHEQUE Biobank (BBMRI, France). All
359 patients gave a specific written informed consent. The study was approved by local Ethics
360 Committee (Advice 20-190-404).

361

362 **Results**

363 GCs ingest apoptotic oocytes and other apoptotic substrates

364 Our first challenge was to ensure that the GC ingest the apoptotic oocytes. Therefore, we
365 incubated the primary culture of human GC with apoptotic oocytes, and then performed IF
366 analysis. We used FITC-labeled oocytes to follow their path after the incubation with cultured
367 primary GC. In parallel experiments we incubated the cells with the isolated fraction of rat POS.

368 Figure 1 a, a', b, and b' shows that primary cultures of human GC interacted with FITC-
369 labeled apoptotic substrates, so that the green-colored points were found in association with the
370 cells. Some green points were located at the cell periphery (the others exhibited peri-nuclear
371 localization. Not only primary cultures of GC, but also human granulosa KGN cell line
372 interacted with apoptotic substrates (apoptotic oocytes, POS or the fragments of apoptotic KGN
373 cells obtained after the induction of apoptosis by ceramide) (Fig.1, c, d; Supplementary Fig.
374 S1a). Figure 1 (c, d) shows green colored fragments of apoptotic substrates in close association
375 with the cultured KGN cells in both the cell periphery and next to the nuclei. Because of the
376 transparency of the plasma membrane, it is often problematic to discern by light microscopy the
377 substrates bound to the plasma membrane and/or ingested by the cells (Yefimova et al., 2018).
378 Therefore, to ensure that apoptotic oocytes and other apoptotic substrates were ingested by the
379 GC, we then proceeded with TEM. TEM analysis allowed us to reveal the fragments of apoptotic
380 oocytes, and other apoptotic substrates (the fragments of apoptotic KGN cells, the POS) in the

Accepted manuscript

381 cytoplasm of cultured GC (Fig.1 e-g). In agreement with our IF data, the fragments of apoptotic
382 substrates were found in the periphery of the GC, enclosed in phagocytic vacuoles (Fig.1 f, g),
383 and more deeply in cell cytoplasm (Fig.1 f, g). Of note that in all cases the ingested apoptotic
384 substrates were enclosed in single-membrane phagosome vacuole.

385 Thus, the cultured GC exhibited the ability to ingest the apoptotic oocytes and other
386 apoptotic substrates. It was then of interest to obtain insights into the molecular mechanisms
387 providing the ingestion and further management of ingested substrates by the GC.

388

389 Incubation of GCs with apoptotic substrates engages phosphorylation of MERTK

390 The primary response of the phagocyte involves the activation of specific receptors,
391 which mediates reorganization of the actin cytoskeleton in order to form a phagocytic cup, and to
392 ingest prey (Yefimova et al., 2018).

393 MERTK mediates the ingestion of apoptotic substrates in the testis and in the retina
394 (Duncan et al., 2003; Yefimova, 2013). Because the isolated fraction of POS is a practical tool to
395 study MERTK activation and LAP engagement in other phagocytic cells (Kim et al., 2013;
396 Yefimova et al., 2013), we first incubated the KGN cells with POS in order to look for the
397 distribution of phosphorylated MERTK. During the classical phagocytosis process, phagocytic
398 cups harboring engulfed substrates co-localize with the activated phagocytosis receptors
399 (Freeman & Grinstein, 2014). Confocal analysis showed that phospho-MERTK clusters did co-
400 localize on the sites of contact of apoptotic substrate with the GC (Fig. 2 a, b). Co-localisation
401 analysis revealed that 58.8±4.1% of substrate co-localized with 54.98±4.5% of clustered
402 phosphorylated receptors (Fig. 2 c).

403 WB analysis confirmed the phosphorylation of MERTK during incubation of KGN cells
404 with the isolated fraction of POS (Fig. 2 d). Remarkably, the incubation of KGN cells with
405 apoptotic oocytes also resulted in MERTK phosphorylation, which gradually increased over time
406 (Fig. 2 e), suggesting the involvement of MERTK in the primary phagocytosis response by KGN

Accepted manuscript

407 cells. Incubation of KGN cells with apoptotic oocytes led to more pronounced phosphorylation
408 of MERTK compared to that with ROS, as shown in the quantification data (Fig. 2 d, e).

409 MERTK signaling results in the recruitment of motor molecule myosin II, which
410 facilitates substrate moving inside the phagocytes (Strick et al., 2009). In phagocytic cells from
411 the retina and testis, this is heralded by the formation of myosin II clumps on the site of contact
412 of phagocyte with prey. Therefore, we then studied the distribution of myosin II in KGN cells
413 exposed to apoptotic substrates. Confocal analysis confirmed the clumping of myosin II on the
414 sites of contact with apoptotic substrates (Fig. 2, f-h). Co-localization analysis showed that
415 67.02±9.82% of myosin II clumps co-localized with the fragments of apoptotic substrates (Fig. 2
416 i). Thus, the data obtained supported implication of the phagocytosis receptor MERTK in the
417 primary phagocytosis response by the GC.

418

419 Uptake of apoptotic substrates but not of inert microspheres involves a fast lipidation of
420 LC3 protein in GC

421 A major difference between LAP and classical phagocytosis is the accumulation of the
422 lipidated form of LC3 protein (LC3-II). A major difference between LAP and conventional
423 autophagy is a very short time taken for the accumulation of LC3–II. (Kim et al., 2013;
424 Klionsky et al., 2016).

425 The uptake of synthetic inert microspheres does not engage LAP in phagocyte cells
426 (Martinez et al., 2011), so that the phagosomes carrying the inert beads fail to contain LC3 and
427 other LAP-related proteins (Martinez et al., 2011). Therefore, we then compared by IF the
428 immunodistribution of LC3 protein in KGN cells fed with the inert fluorescent microspheres or
429 with POS. Figure 3 a, b shows that anti-LC3 antibody stains the cytoplasm and intracellular
430 vesicles in KGN cells. In cells exposed to POS, the green dots corresponding to LC3 protein co-
431 localized with red anti-rhodopsin immunostaining (Fig. 3 a). On the contrary, these green dots

Accepted manuscript

432 were not associated with fluorescent microspheres (Fig. 3 b). This suggests the involvement of
433 LAP in the management of POS, but not of fluorescent beads.

434 Using WB we compared the expression of LC3 protein in the lysates of GC incubated
435 with the inert microspheres and with the POS. Figure 3 c (upper panel, + beads) shows that in the
436 lysates of KGN cells fed with the microspheres, the soluble form of LC3 protein (LC3-I, 17 kDa
437 band) predominated on the blots at all times of incubation. In contrast, in the lysates from the GC
438 incubated with POS (Figure 3 c, upper panel, + POS) a progressive increase of the lipidated form
439 of LC3 protein (LC3-II, 14 kDa) was detected, starting from 30 min of incubation. Such early
440 conversion of LC3-I to LC3-II during the uptake of POS (but not of microspheres) strongly
441 suggests the involvement of LAP in the management of apoptotic substrates by GC. A kinetic
442 study showed an increase of lipidated form of LC3 protein over time (Fig. 3c, bottom panel, left
443 side) during the uptake of POS. The accumulation of LC3-II protein was also detected in GC fed
444 with the fragments of apoptotic oocytes (Fig.3 c, bottom panel, right side). Of note is that the
445 accumulation of LC3-II in cell lysates was associated with the progressive decrease of the
446 intensity of GAPDH band used as housekeeping gene, probably due to the activation of
447 degradation processes. Therefore, in our subsequent kinetic experiments we normalized WB data
448 to time 0 (cells + phagocytosis substrate at the time 0).

449 Confocal microscopy followed by 3D reconstruction revealed LC3 protein on the surface
450 of KGN cells in phagocytic cups containing POS (Fig. 3 d, e, f), and in the cytoplasm of KGN
451 cells together with the ingested fragments of POS (Fig. 3 e, f). Quantitative co-localization
452 analysis showed the partial co-localization of POS with LC3 protein (Fig. 3 g). Thus, 10.6±3.0%
453 of phagocytosis substrates co-localized with 43.1±9.7% of LC3-stained structures (the ratio
454 LC3/substrate = 4.07). Long-term kinetic experiments attested the gradual increase of the
455 lipidation of LC3 protein over time (0-6h), supporting the continuity of the process (Fig. 3 h).

456 We used an antibody against the main protein of the zona pellucida, zona pellucida
457 glycoprotein 3 (ZP3), to immunolocalize the fragments of apoptotic oocytes taken by the GC. As

Accepted manuscript

458 in the previous case (i.e. incubation with POS), anti-LC3 antibody stained phagocytic cups,
459 containing the fragments of apoptotic oocytes, and those ingested by the GC (Fig. 3, i-l). The
460 rapid conversion of LC3-I to LC3-II (starting from 30 min of incubation; Fig. 3 c) and increase
461 in LC3-II/LC3I ratio over time was also detected in the lysates from KGN cells exposed to the
462 fragments of apoptotic oocytes (Fig. 3 m). Collectively these data support the involvement of
463 LAP in the management of apoptotic substrates by the GC.
464

465 Uptake of apoptotic substrates by GC engages autophagy proteins

466 In contrast to classical phagocytosis cups, those formed during LAP contain several
467 autophagy proteins (Kim et al., 2013; Panneerdoss et al., 2017; Duan et al., 2018). Thus, Beclin1
468 and ATG5 proteins are known to be recruited to phagosomal membranes as a very early event in
469 LAP (Martinez et al., 2011; Kim et al., 2013; Li et al., 2013). Therefore, we then investigated the
470 distribution of Beclin1 and ATG5 in human granulosa KGN cells exposed to apoptotic
471 substrates, by confocal immunofluorescent microscopy. We also followed by WB the expression
472 of these proteins in KGN cells during their incubation with apoptotic oocytes and/or with the
473 POS.

474 Figure 4 shows the immunodistribution of ATG5 and Beclin1 proteins in KGN cells,
475 exposed to POS (Fig. 4 a, b, j, k) and to apoptotic oocytes (Fig. 4 e-h, n-q). By confocal analysis
476 we demonstrated that both ATG5 and Beclin1 proteins are present in the cytoplasm of KGN
477 cells, and in association with intracellular vesicles. Confocal slicing and 3D analysis of GC
478 exposed to POS and/or apoptotic oocytes revealed strong co-localisation of apoptotic substrates
479 with autophagy proteins ATG5 and Beclin1 (Fig. 4 a, b, e-h, j, k, n-q). Indeed, ATG5 and Beclin
480 1 co-localized with apoptotic substrates on the surface of KGN cells during the formation of
481 phagocytic cups and after their ingestion in the cytoplasm of KGN cells. This corroborates the
482 contribution of autophagy proteins to the formation and maturation of the phagosome/LAPosome

Accepted manuscript

483 in KGN cells. As showed in control experiments, ATG5 and Beclin 1 proteins did not co-localize
484 with the inert microspheres ingested by KGN cells (Supplementary Fig. S1 b, c).

485 Quantitative co-localization analysis revealed the partial co-localization of phagocytosis
486 substrates with autophagy proteins. Thus, 10.8±1.7% of phagocytosis substrates co-localized
487 with 13.7±6.2% of ATG5-stained vesicles (the ratio ATG5/substrate = 1.26); and 15.9±2.7%
488 phagocytosis substrates co-localized with 31.0±7.2% Beclin1-stained vesicles (the ratio
489 Beclin1/substrate =1.95) (Fig. 4 c, l).

490 We also analyzed the lysates of KGN cells for the presence of ATG5 and Beclin1
491 proteins by WB at different times of incubation with apoptotic oocytes and POS. Both ATG5
492 and Beclin1 proteins were found in the lysates of KGN cells at all times of incubation (from 0h
493 to 6h) (Fig. 4 d, i ,m, r). Densitometry analysis of blots revealed a relative increase of ATG5
494 proteins during the incubation of KGN cells with the apoptotic oocytes (Fig. 4 i), while the
495 expression of Beclin 1 protein did not vary during the same incubation period. We also explored
496 the expression of ATG7 protein, which is specifically involved in LAP (Klionsky et al., 2016).
497 WB analysis shows that KGN cells loaded with apoptotic substrates stably expressed ATG7
498 during the incubation period (Supplementary Fig. S1d). Thus, the uptake of apoptotic substrates
499 by the GC engages autophagy proteins, as occurs after LAP activation.

500

501 Rapamycin treatment slows down the ingestion of apoptotic substrates by GC

502 Phagocytosis, autophagy and LAP utilize lysosomes for cargo degradation (Muniz-
503 Feliciano et al., 2017). In rodent retinal pigment epithelium (RPE) cells under physiological
504 condition, phagocytosis and autophagy processes reach their peak at different times of day. This
505 avoids the competition for lysosomal resources *in vivo* (Muniz-Feliciano et al., 2017) and
506 suggests a balance between autophagy and LAP in phagocytes. Indeed, starvation-induced
507 autophagy impaired the degradation of POS (Kim et al., 2013; Muniz-Feliciano et al., 2017).

Accepted manuscript

508 Therefore, it was of interest to explore whether the induction of autophagy in GC would
509 influence the uptake of apoptotic substrates.

510 Because of the involvement of mTOR (mechanistic target of rapamycin [serine/threonine
511 kinase])-dependent autophagy in follicular development (Choi et al., 2014), we chose rapamycin
512 to induce autophagy in the GC. WB analysis of cell lysates confirmed the lipidation of LC3
513 protein in rapamycin-treated cells (Supplementary Fig. S1 e). Then, we incubated rapamycin-
514 treated and untreated cells with POS and analyzed their distribution using a phagocytosis test,
515 which discriminates between bound and ingested substrates (Yefimova et al., 2013; Yefimova et
516 al., 2018). Figure 4 s (top panel) shows that in control cells the red staining corresponding to
517 POS was mainly associated with small fragments, located in cell cytoplasm. The large fragments
518 of POS, attached to plasma membrane, were less frequent. On the contrary, in rapamycin-treated
519 cells these large fragments of POS predominated (Fig. 4 s, bottom panels). The large fragments
520 of POS strongly colocalized with anti-LC3 immunoreactivity (green). In merged pictures from
521 rapamycin-treated cells (Fig. 4 s, bottom panels) the fragments of POS appeared to be encircled
522 with anti-LC3 immunostaining, suggesting their engulfment in phagocytic cups.

523 As shown in quantification analysis, both control and rapamycin-treated GC
524 progressively accumulated the POS over time (Fig. 4 t). At all times of incubation, the total
525 amount of POS (bound + ingested) associated with KGN cells was similar in rapamycin-treated
526 and untreated specimens (Fig. 4 t). Nevertheless, the phagocytosis test revealed that the amount
527 of ingested POS was dramatically reduced in rapamycin-treated GC compared to control cells.
528 This effect was observed starting from 30 min of incubation and continued at all periods studied
529 (up to 2 hours) (Fig. 4 t). The phagocytosis test supported the data from IF analysis, which
530 attested the predominance of phagocytic cups, but not of intracellular fragments of POS, in
531 rapamycin-treated cells (Fig. 4 s).

532

Accepted manuscript

533 Degradation of apoptotic substrates by GC requires lysosomal proteolysis, but not the
534 depletion of p62 protein

535 Examination of tissue sections shows that phagocytosis of apoptotic substrates by both
536 Sertoli and RPE cells results in an increase in number of lysosomes (Chemes et al., 1986;
537 LaVail, 1976). Therefore, it was then of interest to look at the content of lysosomes in the GC
538 during the uptake of apoptotic oocytes and/or POS using different techniques.

539 We first used a classical Gomori method (Allison & Mallucci, 1969) for acid phosphatase
540 activity to assess lysosomal enzymes cytochemically. Using the cytochemical technique in
541 control GC, lysosomes were identified as brown vesicles of identical size located next to the
542 nucleus (Fig. 5 a). In the absence of phagocytosis each granulosa cell contained on average 9.3 ±
543 0.3 (n=110) Gomori-stained points, so that the ratio of brown-colored area per cell corresponded
544 to a value of = $6.4\ 10^{-4} \pm 0.6\ 10^{-4}$ (n=110). Uptake of either apoptotic oocytes or POS resulted in a
545 dramatic increase of Gomori staining in the GC (Fig. 5 b, c). In both cases, the brown points
546 exhibited a variable size, shape and location in the GC. Some of Gomori-stained vesicles (Fig. 5
547 b, c) concentrated on the cell periphery, while others were detected next to the nucleus, or
548 encircled plasma membrane. Quantification revealed a huge increase in Gomori staining in cells
549 challenged with oocytes and POS (Fig. 5 d, upper panel), which corresponded to the values of
550 $1.1\ 10^{-2} \pm 0.1\ 10^{-2}$ (n=250) and $1.4\ 10^{-2} \pm 0.2\ 10^{-2}$ (n=250), respectively.

551 Cathepsin D is the main lysosomal protease, involved in the degradation of different
552 substrates by various phagocytes, including the Sertoli cells and the RPE cells (Zimmerman et
553 al., 1983; Igdoura et al., 1995; Benes et al., 2008). Cathepsin D is also expressed in the GC.
554 Moreover, its activity increases in the atretic follicles (Dhanasekaran, et al. 1983). Therefore, we
555 then studied the immunodistribution of Cathepsin D in the KGN cells incubated with the POS
556 and with the fragments of apoptotic oocytes.

557 In KGN cells exposed to the fragments of POS, the anti-Cathepsin D immunostaining
558 presented a vesicular pattern, implying association of the protein with the lysosomes (Fig. 5, e-

Accepted manuscript

559 h). Quantification demonstrated that the amount of Cathepsin D-stained vesicles increased over
560 time during the incubation of KGN cells with the POS (Fig. 5 d, lower panel). In KGN cells
561 exposed to apoptotic oocytes, anti-Cathepsin D immunostaining strongly concentrated around
562 the fragments of apoptotic oocytes undergoing the process of the ingestion or which were
563 already ingested by the cell (Fig. 5 i-k). The 3D reconstruction (Fig. 5 k) shows that anti-
564 Cathepsin D immunostaining formed the "coats" encircling the fragments of apoptotic oocytes,
565 which were located on the cell surface and in the cytoplasm (Fig. 5 i-k, lower panels, selections
566 1-4).

567 We examined by WB the content of Cathepsin D in the lysates of KGN cells fed with
568 POS and/or apoptotic oocytes. Cathepsin D is produced in the inactive form, pre-proCathepsin
569 D, which is quickly converted into proCathepsin D (Lai et al., 2000) and then to biologically
570 active Cathepsin D. As usual, both proCathepsin D 56 (kDa) and Cathepsin D are present on the
571 blots from cell lysates in differential proportional relationships (Lai et al., 2000). In our hands,
572 the Cathepsin D from cell lysates of KGN cells migrated as a single band of 34 kDa. We did not
573 detect on the blots an inactive 56 kDa form, probably because of the fast conversion of newly
574 synthesized proCathepsin D in its active form (Fig. 5 l). Of note, is that the proCathepsin D (56
575 kDa) was clearly detected in cell lysates from the human RPE cell line (hTERT-RPE1) incubated
576 with the POS, used as a control (Supplementary Fig. S1 f). In agreement with our quantification
577 study, WB analysis also demonstrated the increase of Cathepsin D content during the incubation
578 of KGN cells with the POS, and with the apoptotic oocytes (Fig. 5 i).

579 Thus, cytochemical, immunocytochemical, and WB experiments revealed an increase of
580 lysosome-related parameters during phagocytosis by GC. Then, TEM examination of ultrathin
581 sections from KGN cells challenged with apoptotic substrates was undertaken. Figure 5 shows
582 that lysosome content (both primary and secondary lysosomes) dramatically increases during the
583 exposure of KGN cell cultures to apoptotic oocytes and POS (Fig. 5 m, n, o). Quantification
584 revealed a 4-fold increase in lysosome content after 12h of phagocytosis of apoptotic substrates

Accepted manuscript

585 by the GC, compared to control (absence of phagocytic substrate) (Fig. 5, p). This is in good
586 agreement with previous results, attesting the contribution of lysosomes to the management of
587 ingested apoptotic substrates.

588 p62 protein is a specific adaptor involved in autophagy. It selectively recognizes
589 autophagic cargo and mediates its engulfment into autophagosomes (Lippai & Lőw, 2014).
590 When lysosome-dependent autophagy degradation is activated the content of p62 decreases,
591 whereas the LAP-dependent degradation does not modify the levels of p62 in the cells (Muniz-
592 Feliciano et al., 2017). Therefore, we then studied by WB the content of p62 protein in KGN
593 cells challenged with POS and/or apoptotic oocytes. WB analysis did not reveal any variation in
594 the content of p62 protein in KGN cells at all times of incubation with POS (Fig. 5 q) or
595 apoptotic oocytes (Fig. 5 r), thereby supporting the involvement of LAP in their degradation.

596 Collectively, we concluded that GC efficiently ingest and degrade apoptotic oocytes and
597 other apoptotic substrates in a process strongly resembling LAP.

598

599 **Discussion**

600 The removal of apoptotic cells and cell debris that are continuously produced during the
601 lifespan of a tissue is a vital task in all tissues of the body (Arandjelovic & Ravichandran, 2015).
602 This task is routinely achieved by professional phagocytes, which are the cells of hematopoietic
603 origin such as macrophages, dendritic cells and microglia. Professional phagocytes ingest and
604 destroy apoptotic substrates in almost all tissues of the body, except the retina and the testis. The
605 retina and the testis, which are isolated from the blood, were classically considered as exceptions
606 to the general rule because the removal of apoptotic substrates was achieved by resident
607 epithelial cells (Nakanishi et al., 2011; Penberthy et al., 2018). Here we demonstrate that the
608 ovary is a third example of a tissue that uses the same principle as retina and the testis to remove
609 apoptotic substrates through the functioning of local epithelial cells.

Accepted manuscript

610 We show here for the first time that human GC maintained *in vitro* (primary culture and
611 KGN cell line) efficiently ingest and destroy apoptotic oocytes. To this end, we show that GC
612 use, in part, the LAP mechanism - a hybrid process in which a classical phagocytosis is
613 supported by autophagy degradation machinery. Being triggered by the uptake of extracellular
614 cargoes, but not by autophagy inducers, LAP is a separate process, which differs from
615 phagocytosis and autophagy in their morphological, molecular and temporal aspects. Therefore,
616 in this work we used different approaches, such as ultrastructure examination, and kinetic and
617 molecular studies, to identify the involvement of LAP in the management of apoptotic substrates.
618 All of these approaches supported the involvement of LAP, but not of autophagy, in the
619 processing of apoptotic substrates by GC.

620 LAP is a tightly regulated mechanism in which the efficacy of substrate clearance
621 determines the rate of the ingestion of apoptotic substrates owing to a regulatory feedback loop
622 (Teplova et al., 2013). In the blood-separated retina and testis, ingestion of apoptotic substrates
623 largely relies upon activation of the phagocytosis receptor MERTK, a member of the TAM
624 (Tyro3, Axl, MERTK) family of tyrosine kinases involved in various aspects of cell life (Lemke
625 & Rothlin, 2008). Being expressed by retinal pigmented epithelial cells and by the somatic
626 Sertoli cells in testis, TAM receptors play a pivotal role for vision and male reproduction
627 function (Duncan et al., 2003; Lemke & Rothlin, 2008). Genetic ablation or mutation of *MERTK*
628 results in irreversible blindness in human and animal models (Duncan et al., 2003). When
629 combined with the mutations in *Tyro3* and *Axl*, triple mutant TAM-/- mice exhibit abnormal
630 spermatogenesis, infertility in males and reduced fertility in females (Lu et al., 1999): the latter
631 observation strongly indicates the importance of TAM receptors in the molecular mechanisms
632 sustaining female fertility. Remarkably, transcriptomic analysis of bovine GC from small antral
633 follicles undergoing atresia revealed a 4-fold increase of MERTK expression (Hatzirodos et al.,
634 2014), supporting the idea of the role of GC in removing apoptotic oocytes.

Accepted manuscript

635 A dysfunction in both the MERTK receptor and LAP mechanism contributes to
636 establishment of the lupus-like autoimmune status associated with sustained inflammation (Scott
637 et al., 2001; Lemke & Rothlin, 2008; Rothlin, et al., 2015; Martinez et al., 2016). Indeed, in
638 normal situations, LAP is a rapid "immunologically silent" process in which the apoptotic
639 substrates are managed at the early stages of apoptosis. However, once the integrity of the
640 plasma membrane is lost due to the secondary necrosis of late-stage apoptotic cells, the released
641 cellular contents can engage receptors for damage-associated molecular patterns and contribute
642 to immune responses to self antigens (Janko et al., 2011; Arandjelovic & Ravichandran, 2015).
643 Remarkably, the human ovary is commonly the target of an autoimmune attack leading to
644 ovarian dysfunction, manifested as premature ovarian failure (POF), polycystic ovary syndrome
645 (PCOS), unexplained infertility, or endometriosis (Komorowska, 2016). In the case of POF, the
646 autoantibodies to ovarian antigens have been clearly documented in numerous studies (Nelson,
647 2009; Gleicher et al., 2015). Besides, inflammation plays a considerable role in the mechanism
648 of POF, and controlling the development of inflammatory status may be one of the methods to
649 treat POF (Huang et al., 2019).

650 One of the major functions ascribed to LAP is to promote phagosome maturation through
651 the recruitment of autophagy proteins (Martinez et al., 2011). However, recent reports suggest
652 that this requirement is not universal. Thus, in mouse embryonic fibroblasts and in bone marrow-
653 derived macrophages, maturation of the phagosome was not affected after ablation of the *ATG5*
654 and *ATG7* genes (Cemma et al., 2016), highlighting the complexity and cell-specificity of LAP
655 in different phagocytosis models. In our KGN cell model, we observed an increase of the
656 expression of ATG5 protein during phagocytosis of apoptotic oocytes, while those of ATG7 did
657 not vary. The formation of phagocytic cups and the ingestion of apoptotic substrates progress
658 through activation of a downstream effector, Ras-related C3 botulinum toxin substrate (RAC1),
659 which mediates actin reorganization (Kim et al., 2013; Teplova et al., 2013; Panneerdoss et al.,
660 2017; Duan et al., 2018). While the order of events in the signaling pathways remains an

Accepted manuscript

661 unaddressed question (Heckmann et al., 2017), the recruitment of autophagy proteins seems to
662 be necessary to sustain MERTK-mediated ingestion. Indeed, the invalidation of *Atg7 and*
663 *Beclin1* genes results in the decreased expression of phagocytosis receptor MERTK and integrin
664 beta5, which co-operate with MERTK to facilitate the ingestion (Teplova et al., 2013).
665 Noteworthy, along with the increase of MERTK (Hatzirodos et al., 2014) GC from the atretic
666 follicles increase the expression of autophagy proteins (Choi et al., 2010), suggesting the co-
667 operation of both partners during the process of atresia. In agreement with these *in vivo*
668 observations are the results from our *in vitro* model, in which the phosphorylation of MERTK
669 and lipidation of LC3 protein progressed over time to provide the ingestion of apoptotic
670 substrates. In fact, the early time-course of LC3 lipidation (starting from 30 min of incubation
671 with apoptotic substrates) is more compatible with the activation of LAP than autophagy in GC.

672 Our data show that the exposure of GC to apoptotic oocytes and/or POS induced a
673 significant increase in lysosome number. Of note is that a strong increase of lysosome quantity
674 also occurs in the Sertoli cells from seminiferous tubules and in RPE cells following
675 phagocytosis of spermatid residual bodies and of POS (Chemes et al., 1986; LaVail, 1976). On
676 the contrary, the activation of autophagy has also been shown to dramatically reduce the number
677 of lysosomes in cells (Xu & Ren, 2015). In line with this, the response of GC fits with a classical
678 response of phagocyte cells, which boost lysosome gene expression and lysosome number to
679 handle successive rounds of phagocytosis (Gray et al., 2016; Wong et al., 2017).

680 Cathepsin D, a key lysosomal protease (Benes at al., 2008), which ensures the
681 degradation of apoptotic substrates in the retina and the testis (Bosch et al., 1993; Saewu et al.,
682 2012), is expressed in GC (Dhanasekaran & Moudgal, 1986). Remarkably, the expression of
683 Cathepsin D increases in GC from early atretic follicles (Dhanasekaran & Moudgal, 1983;
684 Dhanasekaran & Moudgal, 1989). We also detected by WB experiments a progressive increase
685 of Cathepsin D protein in GC exposed to either POS or apoptotic oocytes. One interesting
686 finding was the absence of a protein band corresponding to inactive proCathepsin D 56 (kDa) on

Accepted manuscript

687 the blots from the lysates of GC challenged with phagocytosis substrates, although this band was
688 clearly seen on the blots from the lysates of hTERT-RPE1 cells used as control. This could either
689 indicate some peculiarities in the processing of Cathepsin D, or the rapid conversion of the
690 enzyme from the inactive to active state by GC.

691 Autophagy and LAP are distinct pathways that use many of the same mediators and must
692 compete for cellular resources (Muniz-Feliciano et al., 2017). In agreement with this, in our
693 study we show that the induction of autophagy in GC negatively influences the processing of
694 nascent phagosomes (Lu & Zhou, 2012), as reported for RPE cells (Kim et al., 2013; Muniz-
695 Feliciano et al., 2017). Another reliable criterion to support the involvement of LAP in lysosomal
696 degradation is the level of p62 protein. p62 is a special adaptor for autophagy degradation
697 (Klionsky et al., 2016), therefore the level of p62 decreases when autophagy is activated but
698 remains unchanged during LAP (Muniz-Feliciano et al., 2017). In line with this, our study
699 supports the idea of the involvement of LAP, but not of autophagy, in the degradation of
700 apoptotic substrates ingested by the GC.

701 To date, the information on regulation of LAP is scarce. A study on retinal pigmented
702 epithelial cells demonstrated that autophagy-inducing factors suppress LAP (Muniz-Feliciano et
703 al., 2017). One of these factors is the epidermal growth factor receptor (EGFR), whose activation
704 promotes autophagy and suppresses LAP. EGFR is expressed in GC (Shimada & Yamashita,
705 2011). Furthermore, its activation is induced by FSH, which is a key regulator of folliculogenesis
706 and spermatogenesis (Jégou, 1993; Shimada & Yamashita, 2011). Exogenous FSH is widely
707 used to prevent GC apoptosis and follicular atresia. Moreover, administration of FSH induces
708 autophagy in GC, promoting follicular growth and development (Zhou et al., 2017), but not
709 atresia. On the other hand, a study of the seminiferous tubules demonstrated an inhibitory effect
710 of FSH on the ingestion of apoptotic substrates by the Sertoli cells (Pineau et al., 1991). Overall,
711 these data give some indirect indications of the possible role of FSH in the regulation of LAP-

Accepted manuscript

712 dependent removal of apoptotic oocytes by the GC, opening a new view on the treatment of POF
713 and PCOS.

714 In summary, here we demonstrate for the first time that blood-barrier forming epithelial
715 GC can act as powerful non-professional phagocytes in maintaining ovarian homeostasis. This is
716 achieved through the removal from ovarian tissue of apoptotic substrates by means of
717 unconventional autophagy-assisted phagocytosis. Cleaning of apoptotic oocytes by the
718 surrounding GC seems likely to be a physiological mechanism involved in follicular atresia. A
719 better understanding of this physiological process could open new strategies in the treatment of
720 ovarian dysfunctions associated with the imbalanced content of germ cells in the ovaries, such as
721 POF and/or PCOS.

722

723

724 **Acknowledgments**

725 We thank Dr. A Cantereau-Becq for confocal imaging, Mr. A Dupont and Mr. G
726 Gukasyan for excellent technical assistance. We thank Prof. V Catros and Dr. JC Hervé for
727 critical reading of the manuscript. We thank H2P2 platform and MRIC platform from Rennes
728 University, and Image UP platform from Poitiers University. MGY was welcomed as invited
729 Professor by CHU de Rennes. MGY acknowledges Direction de la Recherche Clinique du CHU
730 de Rennes.

731

732 **Authors' roles**

733 MGY carried out study design, execution, analysis of data, and writing/revising the
734 manuscript. CL and ACM participated in human granulosa cell collection and
735 immunocytochemistry experiments. ABurel and MTL participated in electron microscopy
736 experiments. ABashamboo and CE participated in primary culture setting up. CP, SV, ASN and
737 SJ recruited IVF samples. BJ participated in the structuration of the team research funding and

Accepted manuscript

manuscript revision. NB was involved in study conception, data analysis, and manuscript revision. CR is the senior author involved in study conception, data analysis, and manuscript revision. All authors read and approved the final manuscript.

Funding

The study was funded by Rennes Metropole (AIS 2015) and Agence de BioMédecine. This work was supported by funding from Université de Rennes1, Institut National de la Santé et de la Recherche Médicale (INSERM) and CHU de Rennes. A. Bashamboo is funded in part by the program Actions Concertees Interpasteuriennes (ACIP) and a research grant from the European Society of Pediatric Endocrinology. This work is supported by the Agence Nationale de la Recherche Grants ANR-17-CE14-0038 and ANR-10-LABX-73.

Conflict of interest

None declared.

References

Allison AC, Mallucci I. Histochemical studies of lysosomes and lysosomal enzymes in virus-infected cell cultures. *J Exp Med* 1965;**121**:463-476.

Amer AO, Swanson MS. Autophagy is an immediate macrophage response to Legionella pneumophila. *Cell Microbiol* 2005;**7**:765-78.

Arandjelovic S, Ravichandran KS. Phagocytosis of apoptotic cells in homeostasis. *Nat Immunol* 2015;**16**:907-917.

Accepted manuscript

761 Bandyopadhyay U, Overholtzer M. LAP: the protector against autoimmunity. *Cell Res*
762 2016;**26**:865–866.

763 Benes P, Vetvicka V, Fusek M. Cathepsin D-many functions of one aspartic protease. *Crit*
764 *Rev Oncol Hematol* 2008;**68**:12-28.

765 Bosch E, Horwitz J, Bok D. Phagocytosis of outer segments by retinal pigment epithelium:
766 phagosome-lysosome interaction. *J Histochem Cytochem* 1993;**41**:253-263.

767 Cemma M, Grinstein S, Brumell JH. Autophagy proteins are not universally required for
768 phagosome maturation. *Autophagy* 2016;**12**:1440–1446.

769 Chemes H. The phagocytic function of Sertoli cells: a morphological, biochemical, and
770 endocrinological study of lysosomes and acid phosphatase localization in the rat testis.
771 *Endocrinology* 1986;**119**:1673-1681.

772 Choi J, Jo M, Lee E, Choi D. AKT is involved in granulosa cell autophagy regulation via
773 mTOR signaling during rat follicular development and atresia. *Reproduction* 2013;**147**:73–
774 80.

775 Choi JY, Jo MW, Lee EY, Yoon BK, Choi DS. The role of autophagy in follicular
776 development and atresia in rat granulosa cells. *Fertil Steril* 2010;**93**:2532-2537.

777 Davis MA, Flaws JA, Young M, Collins K, Colburn NH. Effect of ceramide on intracellular
778 glutathione determines apoptotic or necrotic cell death of JB6 tumor cells. *Toxicol Sci*
779 2000;**53**:48-55.

780 Dhanasekaran N, Moudgal NR. Studies on follicular atresia: role of tropic hormone and
781 steroids in regulating cathepsin-D activity of preantral follicles of the immature rat. *Mol Cell*
782 *Endocrinol* 1986;**63**:133-142.

Accepted manuscript

783 Dhanasekaran N, Moudgal NR. Studies on follicular atresia: role of gonadotropins and
784 gonadal steroids in regulating cathepsin-D activity of preovulatory follicles in the rat. *Mol*
785 *Cell Endocrinol* 1989;**63**:133–142.

786 Dhanasekaran N, Sheela Rani CS, Moudgal NR. Studies on follicular atresia: lysosomal
787 enzyme activity and gonadotropin receptors of granulosa cells following administration or
788 withdrawal of gonadotropins in the rat. *Mol Cell Endocrinol* 1983;**33**:97-112.

789 Duan Z, Chen Q, Du L, Tong J, Xu S, Zeng R, Ma Y, Chen X, Li M. Phagocytosis of
790 *Candida albicans* Inhibits Autophagic Flux in Macrophages. *Oxid Med Cell Longev*
791 2018;**2018**:4938649

792 Duncan JL, LaVail MM, Yasumura D, Matthes MT, Yang H, Trautmann N, Chappelow AV,
793 Feng W, Earp HS, Matsushima GK, Vollrath D. An RCS-like retinal dystrophy phenotype in
794 mer knockout mice. *Invest Ophthalmol Vis Sci* 2003;**44**:826-838.

795 Elmore S. Apoptosis: a review of programmed cell death. *Toxicol Pathol* 2007;**35**:495-516.

796 Finnemann SC, Bonilha VL, Marmorstein AD, Rodriguez-Boulan E. Phagocytosis of rod
797 outer segments by retinal pigment epithelial cells requires alpha(v)beta5 integrin for binding
798 but not for internalization. *Proc Natl Acad Sci U S A* 1997;**94**:12932-12937.

799 Freeman SA, Grinstein S. Phagocytosis: receptors, signal integration, and the cytoskeleton.
800 Immunol Rev 2014;**262**:193-215.

801 Gaytán F, Morales C, Bellido C, Aguilar E, Sánchez-Criado JE. Ovarian follicle
802 macrophages: is follicular atresia in the immature rat a macrophage-mediated event? *Biol*
803 *Reprod* 1998;**58**:52-59.

Accepted manuscript

804 Gleicher N, Kushnir VA, Barad DH. Prospectively assessing risk for premature ovarian
805 senescence in young females: a new paradigm. *Reprod Biol Endocrinol* 2015;**13**:34.

806 Gray MA, Choy CH, Dayam RM, Ospina-Escobar E, Somerville A, Xiao X, Ferguson SM,
807 Botelho RJ. Phagocytosis Enhances Lysosomal and Bactericidal Properties by Activating the
808 Transcription Factor TFEB. *CurrBiol* 2016;**26**:1955-1964.

809 Hatzirodos N, Hummitzsch K, Irving-Rodgers HF, Harland ML, Morris SE, Rodgers RJ.
810 Transcriptome profiling of granulosa cells from bovine ovarian follicles during atresia. *BMC*
811 *Genomics* 2014;**15**:40.

812 Heckmann BL, Boada-Romero E, Cunha LD, Magne J, Green DR. LC3-Associated
813 Phagocytosis and Inflammation. *J Mol Biol* 2017;**429**:3561-3576.

814 Huang Y, Hu C, Ye H, Luo R, Fu X, Li X, Huang J, Chen W, Zheng Y. Inflamm-Aging: A
815 New Mechanism Affecting Premature Ovarian Insufficiency. *J Immunol Res*
816 2019;**2019**:8069898.

817 Igdoura SA, Morales CR, Hermo L. Differential expression of cathepsins B and D in testis
818 and epididymis of adult rats. *J Histochem Cytochem*1995;**43**:545-557.

819 Itoh M, Yano A, Li X, Miyamoto K, Takeuchi Y. Limited uptake of foreign materials by
820 resident macrophages in murine ovarian tissues. *J Reprod Immunol* 1999;**43**:55-66.

821 Janko C, Franz S, Munoz LE, Siebig S, Winkler S, Schett G, Lauber K, Sheriff A, van der
822 Vlag J, Herrmann M. CRP/anti-CRPantibodies assembly on the surfaces of cell remnants
823 switches their phagocytic clearance toward inflammation. *Front Immunol* 2011;**2**:70.

824 Jégou B. The Sertoli-germ cell communication network in mammals. *Int Rev Cytol*
825 1993;**147**:25–96.

Accepted manuscript

826 Johnston RB Jr, Klemperer MR, Alper CA, Rosen FS. The enhancement of bacterial
827 phagocytosis by serum. The role of complement components and two cofactors. *J Exp Med*
828 1969;**129**:1275-1290.

829 Jungheim ES, Meyer MF, Broughton DE. Best practices for controlled ovarian stimulation in
830 in vitro fertilization. *Semin Reprod Med* 2015;**33**:77-82.

831 Kasuya K. Elimination of apoptotic granulosa cells by intact granulosa cells and
832 macrophages in atretic mature follicles of the guinea pig ovary. *Arch Histol Cytol*
833 1997;**60**:175-184.

834 Katabushi H, Fukumatsu Y, Araki M, Suenaga Y, Ohtake H, Okamura H. Role of
835 macrophages in ovarian follicular development. *Horm Res* 1996;**46** Suppl 1:45-51.

836 Kerr JFR, Wyllie AH, Currie AR. Apoptosis: a basic biological phenomenon with wide-
837 ranging implications in tissue kinetics. *Br J Cancer* 1972;**26**:239 –257.

838 Kim JY, Zhao H, Martinez J, Doggett TA, Kolesnikov AV, Tang PH, Ablonczy Z, Chan CC,
839 Zhou Z, Green DR, Ferguson TA. Noncanonical autophagy promotes the visual cycle. *Cell*
840 2013;**154**:365-376.

841 Klionsky DJ, Abdelmohsen K, Abe A, Abedin MJ, Abeliovich H, Acevedo Arozena A, et al.
842 Guidelines for the use and interpretation of assays for monitoring autophagy (3rd edition).
843 *Autophagy* 2016;**12**:1-222.

844 Komorowska B. Autoimmune premature ovarian failure. *Menopause Rev* 2016;**15**:210-214.

845 Lai CM, Robertson T, Papadimitriou J, Shen WY, Daw N, Constable IJ, Rakoczy
846 PE.Controlled production of active cathepsin D in retinal pigment epithelial cells following
847 adenovirus-mediated gene delivery.*MolTher* 2000;**2**:476-484.

Accepted manuscript

848 LaVail MM. Rod outer segment disk shedding in rat retina: relationship to cyclic lighting.
849 *Science* 1976;**194**:1071–1074.

850 Lemke G, Rothlin CV. Immunobiology of the TAM receptors. *Nat Rev Immunol*
851 2008;**8**:327–336.

852 Li X, Prescott M, Adler B, Boyce JD, Devenish RJ. Beclin 1 is required for starvation-
853 enhanced, but not rapamycin-enhanced, LC3-associated phagocytosis of Burkholderia
854 pseudomallei in RAW 264.7 cells. *Infect Immun* 2013;**81**:271–277.

855 Lippai M, Lőw P. The role of the selective adaptor p62 and ubiquitin-like proteins in
856 autophagy. *Biomed Res Int* 2014;**2014**:832704.

857 Lu N, Zhou Z. Membrane trafficking and phagosome maturation during the clearance of
858 apoptotic cells. *Int Rev Cell Mol Biol* 2012;**293**:269–309.

859 Lu Q, Gore M, Zhang Q, Camenisch T, Boast S, Casagranda F, Lai C, Skinner MK, Klein R,
860 Matsushima GK, et al. Tyro-3 family receptors are essential regulators of mammalian
861 spermatogenesis. *Nature* 1999;**398**:723-728.

862 Martinez J, Almendinger J, Oberst A, Ness R, Dillon CP, Fitzgerald P, Hengartner MO,
863 Green DR. Microtubule-associated protein 1 light chain 3 alpha (LC3)-associated
864 phagocytosis is required for the efficient clearance of dead cells. Proc Natl Acad Sci U S A
865 2011;**108**:17396-17401.

866 Martinez J, Cunha LD, Park S, Yang M, Lu Q, Orchard R, et al. Noncanonical autophagy
867 inhibits the autoinflammatory, lupus-like response to dying cells. *Nature* 2016;**533**:115-119.

868 Martinez J, Malireddi RK, Lu Q, Cunha LD, Pelletier S, Gingras S, Orchard R, Guan JL, Tan
869 H, Peng J, Kanneganti TD, Virgin HW, Green DR. Molecular characterization of LC3-

Accepted manuscript

870 associated phagocytosis reveals distinct roles for Rubicon, NOX2 and autophagy proteins.
871 Nat Cell Biol 2015;**17**:893-906.

872 Masud S, Prajsnar TK, Torraca V, Lamers GEM, Benning M, Van Der Vaart M, Meijer AH.
873 Macrophages target Salmonella by LC3-associated phagocytosis in a systemic infection
874 model. Autophagy 2019;**15**:796-812.

875 Matsuda F, Inoue N, Manabe N, Ohkura S. Follicular growth and atresia in mammalian
876 ovaries: regulation by survival and death of granulosa cells. *J Reprod Dev* 2012;**58**:44-50.
877 Mizushima N, Levine B, Cuervo AM, Klionsky DJ. Autophagy fights disease through
878 cellular self-digestion. *Nature* 2008;**451**:1069-1075.
879 Mizushima N, Yoshimori T, Ohsumi Y. The role of Atg proteins in autophagosome
880 formation. *Ann Rev Cell Dev Biol* 2011;**27**:107-132.

881 Mork L, Maatouk DM, McMahon JA, Guo JJ, Zhang P, McMahon AP, Capel B. Temporal
882 differences in granulosa cell specification in the ovary reflect distinct follicle fates in mice.
883 *Biol Reprod* 2012;**86**:37.

884 Muniz-Feliciano L, Doggett TA, Zhou Z, Ferguson TA. RUBCN/rubicon and EGFR regulate
885 lysosomal degradative processes in the retinal pigment epithelium (RPE) of the eye.
886 *Autophagy* 2017;**13**:2072-2085.

887 Nakanishi Y, Nagaosa K, Shiratsuchi A. Phagocytic removal of cells that have become
888 unwanted: implications for animal development and tissue homeostasis. *Dev Growth Differ*
889 2011;**53**:149-160.

890 Nelson LM. Clinical practice. Primary ovarian insufficiency. *N Engl J Med* 2009;**360**:606-
891 614.

Accepted manuscript

892 Ono Y, Nagai M, Yoshino O, Koga K, Nawaz A, Hatta H, Nishizono H, Izumi G,
893 Nakashima A, Imura J, Tobe K, Fujii T, Osuga Y, Saito S. CD11c+ M1-like macrophages
894 (MΦs) but not CD206+ M2-like MΦ are involved in folliculogenesis in mice ovary. *Sci Rep*
895 2018;**8**:8171.

896 Panneerdoss S, Viswanadhapalli S, Abdelfattah N, Onyeagucha BC, Timilsina S,
897 Mohammad TA, Chen Y, Drake M, Vuori K, Kumar TR, Rao MK. Cross-talk between miR-
898 471-5p and autophagy component proteins regulates LC3-associated phagocytosis (LAP) of
899 apoptotic germ cells. *Nat Commun* 2017;**8**:598.

900 Penberthy KK, Lysiak JJ, Ravichandran KS. Rethinking Phagocytes: Clues from the Retina
901 and Testes. *Trends Cell Biol* 2018;**28**:317-327.

902 Pineau C, Le Magueresse B, Courtens JL, Jégou B. Study in vitro of the phagocytic function
903 of Sertoli cells in the rat. *Cell Tissue Res* 1991;**264**:589-598.

904 Rothlin CV, Carrera-Silva EA, Bosurgi L, Ghosh S. TAM receptor signaling in immune
905 homeostasis. *Annu Rev Immunol* 2015;**33**:355-391.

906 Saewu A, Asuvapongpatana S, Chotwiwatthanakun C, Tantiwongse A, Weerachatyanukul
907 W, Thitilertdecha S. CathepsinD in human reproductive tissues: cellular localization in testis
908 and epididymis and surface distribution in different sperm conditions. *J Androl* 2012;**33**:726-
909 734.

910 Sanjuan MA, Dillon CP, Tait SW, Moshiach S, Dorsey F, Connell S, Komatsu M, Tanaka K,
911 Cleveland JL, Withoff S, Green DR. Toll-like receptor signalling in macrophages links the
912 autophagy pathway to phagocytosis. *Nature* 2007;**450**:1253-1257.

Accepted manuscript

913 Scott RS, McMahon EJ, Pop SM, Reap EA, Caricchio R, Cohen PL, Earp HS, Matsushima
914 GK. Phagocytosis and clearance of apoptotic cells is mediated by MER. *Nature*
915 2001;**411**:207-211.

916 Shaha C, Tripathi R, Mishra DP. Male germ cell apoptosis: regulation and biology. *Philos*
917 *Trans R Soc Lond B Biol Sci* 2010;**365**:1501-1515.

918 Shimada M, Yamashita Y. The key signaling cascades in granulosa cells during follicular
919 development and ovulation process. *J Mamm Ova Res* 2011;**28**:25–31.

920 Siu MK, Cheng CY. The blood-follicle barrier (BFB) in disease and in ovarian function. *Adv*
921 *Exp Med Biol* 2012;**763**:186-192.

922 Strick DJ, Feng W, Vollrath D. MERTK drives myosin II redistribution during retinal
923 pigment epithelial phagocytosis. *Invest Ophthalmol Vis Sci* 2009;**50**:2427-2435.

924 Teplova I, Lozy F, Price S, Singh S, Barnard N, Cardiff RD, Birge RB, Karantza V. ATG
925 proteins mediate efferocytosis and suppress inflammation in mammary involution.
926 *Autophagy* 2013;**9**:459-475.

927 Wirawan E, Lippens S, Vanden Berghe T, Romagnoli A, Fimia GM, Piacentini M,
928 Vandenabeele P. Beclin1: a role in membrane dynamics and beyond. Autophagy 2012;**8**:6-
929 17.

930 Wong CO, Gregory S, Hu H, Chao Y, Sepúlveda VE, He Y, Li-Kroeger D, Goldman WE,
931 Bellen HJ, Venkatachalam K. Lysosomal Degradation Is Required for Sustained
932 Phagocytosis of Bacteria by Macrophages. *Cell Host Microbe* 2017;**21**:719-730.

933 Wu R, Van der Hoek KH, Ryan NK, Norman RJ, Robker RL. Macrophage contributions to
934 ovarian function. *Hum Reprod Update* 2004;**10**:119-133.

Accepted manuscript

935 Wu Y, Tibrewal N, Birge RB. Phosphatidylserine recognition by phagocytes: a view to a kill.
936 *Trends Cell Biol* 2006;**16**:189-197.

937 Xu H, Ren D. Lysosomal physiology. *Annu Rev Physiol* 2015;**77**:57–80.

938 Yadav PK, Tiwari M, Gupta A, Sharma A, Prasad S, Pandey AN, Chaube SK. Germ cell
939 depletion from mammalian ovary: possible involvement of apoptosis and autophagy. *J*
940 *Biomed Sci* 2018;**25**:36.

941 Yefimova MG, Messaddeq N, Harnois T, Meunier AC, Clarhaut J, Noblanc A, Weickert JL,
942 Cantereau A, Philippe M, Bourmeyster N, Benzakour O. A chimerical phagocytosis model
943 reveals the recruitment by Sertoli cells of autophagy for the degradation of ingested
944 illegitimate substrates. *Autophagy* 2013;**9**:653-666.

945 Yefimova MG, Messaddeq N, Meunier AC, Cantereau A, Jégou B, Bourmeyster N.
946 Phagocytosis by Sertoli Cells: Analysis of Main Phagocytosis Steps by Confocal and
947 Electron Microscopy. *Methods Mol Biol* 2018;**1748**:85-101.

948 Yefimova MG, Sow A, Fontaine I, Guilleminot V, Martinat N, Crepieux P, Canepa S,
949 Maurel MC, Fouchécourt S, Reiter E, Benzakour O, Guillou F. Dimeric transferrin inhibits
950 phagocytosis of residual bodies by testicular rat Sertoli cells. *Biol Reprod* 2008;**78**:697-704.

951 Yin Z, Pascual C, Klionsky DJ. Autophagy: machinery and regulation. *Microb Cell*
952 2016;**3**:588-596.

953 Zhou J, Yao W, Li C, Wu W, Li Q, Liu H. Administration of follicle-stimulating hormone
954 induces autophagy via upregulation of HIF-1α in mouse granulosa cells. *Cell Death Dis*
955 2017;**8**:e3001.

Accepted manuscript

956 Zimmerman WF, Godchaux W 3rd, Belkin M. The relative proportions of lysosomal enzyme
957 activities in bovine retinal pigment epithelium. *Exp Eye Res* 1983;**36**:151-158.

958

959 **Figure legends**

960 **Figure 1** Human granulosa cells ingest the apoptotic substrates.

961 (**a-d**) Immunoflourescence (IF) pictures of the primary cultures of human granulosa cells
962 (GC) (**a, a', b, b'**) and human granulosa KGN cell line (**c, d**) incubated with apoptotic oocytes
963 labeled with fluorescein isothiocyanate (FITC) (**a, a', c**), FITC-labeled photoreceptor outer
964 segments (POS) (**b, b'**) and FITC-labeled fragments of apoptotic KGN cells (**d**). Note the green-
965 labeled fragments in cell periphery (arrow) and close to the nucleus stained with 4', 6 diamidino-
966 2-phenylindol (DAPI) (arrowhead). **a'**and **b'** are the merged images of **a** and **b** with DIC
967 projection. (**e, f, g**) Electron micrographs of human granulosa KGN cell line incubated with POS
968 (**e**) with apoptotic oocytes (**f**), and with the fragments of apoptotic KGN (**g**) cells. Note the
969 presence of apoptotic substrates inside the cells close to the plasma membrane (arrow) and more
970 deeply next to the nucleus (n) (arrowhead).

971

972 **Figure 2** Primary phagocytosis response of human GC engages phosphorylation of c-mer proto-
973 oncogene tyrosine kinase and myosin II clumping.

974 Confocal pictures of the human granulosa KGN cells **(a, b, f-h)** challenged with POS. **(a,**
975 **b)** immunostaining with anti-phospho c-mer proto-oncogene tyrosine kinase (MERTK)* (green),
976 and anti-rhodopsin (Rho) antibodies (red); **(b)** is a confocal microscopy slicing of the selected
977 area from **(a)**. Nuclei are stained with DAPI. **(c)** A co-localization diagram (upper panel) and
978 histogram (lower panel), showing the partial co-localization of anti-phospho MERTK* and anti-
979 Rho immunostaining. **(d, e)** Western blotting analysis of MERTK phosphorylation during the
980 exposure of KGN cells to either POS **(d)** or apoptotic oocytes **(e)** with a graph representing

Accepted manuscript

981 MERTK phosphorylation over time normalized to phospho-MERTK* level at time 0; **P <
982 0.001 by ANOVA test with Bonferroni post hoc analysis. **(f-h)** Immunostaining with anti-
983 myosin II (Myo II) (green) and anti-Rho (red) antibodies **(f, g, h)** or with anti-Rho (red)
984 antibodies **(f')**. **(g)** Is a 3D reconstruction of **(f)**. **(h)** A selected area from **(g)** showing the fine
985 structure of Myo II clump containing the POS (double immunostaining, top panel), and after the
986 omission of anti-Myo II (middle panel) and anti-Rho (bottom panel) immunostaining. Nuclei are
987 stained with DAPI. **(i)** Co-localization diagram (upper panel) and histogram (lower panel),
988 showing the partial co-localization of anti-Myo II and anti-Rho immunostaining..
989

990 **Figure 3** Uptake of apoptotic substrates but not of inert microspheres results in the lipidation of
991 microtubule-associated protein 1 light chain 3 protein.

992 (**a, b**) IF pictures of the human granulosa KGN cells challenged with POS **(a)** and
993 fluorescent microspheres/beads (red) **(b).** Immunostaining with anti-Rho (red) **(a)** and with anti-
994 light chain 3 (LC3) (green) **(a, b)** antibodies. Arrows in **(a, b,** left panels**)** denote LC3-labeled
995 dots, asterisks (*) in **a**, (right panel**)** mark co-localization sites of anti-LC3 and anti-Rho
996 immunoreactivity. The nuclei are stained with DAPI. **(c)** Western blotting analysis of LC3-I and
997 LC3-II protein content during exposure of KGN cells to fluorescent microspheres (beads) (upper
998 panel), POS (upper panel and bottom panel, on the left), and apoptotic oocytes (bottom panel, on
999 the right). Note the gradual decrease of housekeeping gene GAPDH during the incubation of
1000 cells with apoptotic substrates. MW: molecular weight markers. **(d)** Confocal picture of KGN
1001 cells challenged with POS after staining with anti-LC3 (green) and anti-Rho (red) antibodies. **(e)**
1002 A 3D reconstruction of **(d). (f)** A selection from **(e)**, in which anti-LC3 (upper panel) or anti-Rho
1003 (lower panel) staining were omitted for better visualization of structures of interest. Confocal
1004 microscopy slicing (**d,** right and lower panels) denotes LC3-stained fragment of POS in cell
1005 cytoplasm (asterisk(*)). Arrow shows nascent phagocytic cup co-stained with anti-LC3
1006 antibodies. **(g)** A co-localization diagram (upper panel) and histogram (lower panel), showing

Accepted manuscript

1007 the partial co-localization of anti-LC3 and anti-Rho immunostaining. **(h)** Western blotting
1008 analysis of LC3-I and LC3-II protein content during exposure of KGN cells to POS with a graph
1009 representing the ratio of LC3-II/LC3-I over time; **P < 0.001 by ANOVA test with Bonferroni
1010 post hoc analysis. **(i, j)** KGN cells challenged with apoptotic oocytes, stained with anti-LC3 (red)
1011 and anti- zona pellucida glycoprotein 3 (ZP3) (green) antibodies. **(j)** Confocal microscopy slicing
1012 of the selected area from **(i)**. In **(j)** DAPI staining is omitted to better visualize the phagocytic
1013 cup at the surface of KGN cell, engulfing the fragment of an apoptotic oocyte (arrows) stained
1014 with anti ZP3-antibodies, and intracellular vacuole stained with anti-LC3 antibodies which
1015 shows very faint anti-ZP3 immunoreactivity (asterisk (*)). **(k)** A 3D reconstruction of **(i)**. **(l)**
1016 Selection from **(k)**, with the omission of DAPI staining (upper panel) or DAPI and ZP3 (green)
1017 staining (lower panel) to better visualize the structure of the phagocytic cup (arrow) and
1018 phagosome (asterisk). **(m)** Western blotting analysis of LC3-I and LC3-II protein content during
1019 exposure of KGN cells to apoptotic oocytes with a graph representing the ratio of LC3-II/LC3-I
1020 over time; **P < 0.001 by ANOVA test with Bonferroni post hoc analysis.
1021
1022
1023 **Figure 4** Ingestion of apoptotic oocytes by human GC engages autophagy proteins.
1024 Confocal pictures of the human granulosa KGN cells **(a, b, e-h, j, k, n-q)** challenged with
1025 POS **(a, b, j, k)** or FITC-labeled **(e-h)** and unlabeled **(n-q)** oocytes. **(a, b)** Immunostaining with
1026 anti- autophagy related protein 5 (ATG5) (green) antibodies. Confocal section (**a**) and 3D
1027 reconstruction (**b**) show green-labeled phagocytic cup (arrow) on the surface of KGN cell co-
1028 stained with anti-Rho antibodies (red). Right panels in **(b)** are the selected area from the left
1029 panel, in which anti-ATG5 (upper panel) or anti-Rho (lower panel) staining were omitted for
1030 better visualization of structures of interest. Asterisk (*) denotes a small anti-ATG5-stained
1031 vesicle, co-stained with anti-Rho antibodies in cell cytoplasm. Nuclei are stained with DAPI. **(c)**
1032 A co-localization diagram (upper panel) and histogram (lower panel), showing the partial co-

Accepted manuscript

1033 localization of anti-ATG5 and anti-Rho immunostaining. **(d)** Western blotting analysis of ATG5
1034 content during exposure of KGN cells to POS with a graph representing ATG5 content over
1035 time, normalized to ATG5 level at time 0, with no significant differences by ANOVA test with
1036 Bonferroni post hoc analysis. **(e-h)** KGN cells challenged with FITC-labeled apoptotic oocytes.
1037 Immunostaining with anti-ATG5 (red) antibodies. Note that the FITC-labeled fragment from the
1038 preparation of apoptotic oocytes is stained with DAPI (confocal microscopy slicing (**e**, right
1039 panels)). **(f)** A 3D reconstruction of the selected area from **(e)**, anti-ATG5 (red) or FITC (green)
1040 staining were omitted from **(g)** and **(h)** panels respectively. Asterisk (*) denotes the intracellular
1041 fragment of FITC-labeled apoptotic oocyte (green), enclosed in a vacuole stained with anti-
1042 ATG5 antibodies (red). **(i)** Western blotting analysis of ATG5 content during exposure of KGN
1043 cells to apoptotic oocytes with a graph representing ATG5 content over time, normalized to
1044 ATG5 level at time 0; **$P < 0.001$ by ANOVA test with Bonferroni post hoc analysis. **(j, k)**
1045 KGN cells challenged with POS. Immunostaining with anti-Beclin1 (Bcn1) (green) antibody and
1046 anti-Rho (red) antibody. Confocal section (**j**) and 3D reconstruction (**k**) show phagocytic cup
1047 (arrow) on the surface of a KGN cell. Right panels in **(k)** are the selected area from the left
1048 panel, in which anti-Rho (upper panel) or anti-Bcn1 (lower panel) staining were omitted for
1049 better visualization of structures of interest. Nuclei are stained with DAPI. **(l)** A co-localization
1050 diagram (upper panel) and histogram (lower panel), showing the partial co-localization of anti-
1051 Bcn1 and anti-Rho immunostaining. **(m)** Western blotting analysis of Bcn1 content during
1052 exposure of KGN cells to POS with a graph representing Bcn1 content over time, normalized to
1053 Bcn1 level at time 0; with no significant differences by ANOVA test with Bonferroni post hoc
1054 analysis. **(n-q)** KGN cells challenged with apoptotic oocytes. Immunostaining with anti-Bcn1
1055 (red) and anti-ZP3 (green) antibodies. **(o)** A 3D reconstruction of the selection from **(n)**. In **(p, q)**
1056 anti-Bcn1 **(p)** and anti-ZP3 **(q)** staining were omitted for better visualization of structures of
1057 interest. Asterisk (*) denotes a fragment of apoptotic oocyte, labeled by anti-ZP3 antibody
1058 (green), enclosed in a vacuole stained with anti-Bcn1 antibodies (red). **(r)** Western blotting

Accepted manuscript

1059 analysis of Bcn1 content during exposure of KGN cells to apoptotic oocytes with a graph
1060 representing Bcn1 content over time, normalized to Bcn1 level at time 0, with no significant
1061 differences by ANOVA test with Bonferroni post hoc analysis. **(s, t)** Phagocytosis by KGN cells
1062 after rapamycin treatment. **(s)** IF pictures of control (upper panels) and rapamycin-treated (lower
1063 panels) KGN cells after 2 h exposure to POS. Immunostaining with anti-Rho (red) and anti-LC3
1064 (green) antibodies. Arrows indicate the small fragments of POS. Asterisks (*) denote the large
1065 fragments of POS, associated with the plasma membrane of KGN cells. **(t)** Depicts a quantitative
1066 analysis of bound and total (bound + ingested) POS associated with KGN cells. Left histogram:
1067 phagocytosis index for control KGN cell cultures challenged with POS. Right histogram:
1068 phagocytosis index for KGN cell cultures pretreated with 200 nM rapamycin for 24 h. **P <
1069 0.001 by ANOVA with Bonferroni post-hoc analysis.
1070
1071
1072 **Figure 5** Degradation of ingested apoptotic substrates by human GC requires lysosomal
1073 proteolysis.
1074 Gomori staining **(a, b, c)** for acid phosphatase (brown dots) in control GC **(a,** black
1075 arrows**)** and after incubation with apoptotic oocytes **(b)** and POS **(c)**. In **(b, c)** black arrows
1076 denote Gomori staining in cell periphery, white arrows denote brown dots encircling plasma
1077 membrane, white asterisks (*) denote Gomori staining next to cell nucleus. **(d, upper panel)**
1078 Histogram showing the total area of brown dots/per cell during phagocytosis of apoptotic
1079 oocytes and POS. **P < 0.001 by ANOVA test with Bonferroni post hoc analysis. Confocal
1080 pictures **(e, i, j)** and 3D reconstructions **(f, g, h, k)** of the human granulosa KGN cells challenged
1081 with POS **(e-h)** or with the fragments of apoptotic oocytes **(i-k)**. **(e-h)** Immunostaining with anti-
1082 Cathepsin D (CatD) antibodies (green) at different times of incubation (2 **(e, f),** 4 **(g)**, 6 **(h)**
1083 hours) with POS (anti-Rho immunostaining (red)). **(f)** A 3D reconstruction of **(e).** Note the
1084 vesicular pattern of anti-CatD immunostaining. Nuclei are stained with DAPI. **(d, lower panel)**

Accepted manuscript

1085 Histogram showing the total area of vesicles stained with anti-CatD antibodies/per cell nuclei
1086 during phagocytosis of POS. **P < 0.001 by ANOVA test with Bonferroni post hoc analysis. **(i,**
1087 **j, k)** Confocal pictures and 3D reconstruction **(k)** of KGN cells challenged with the fragments of
1088 apoptotic oocytes. Ocher is immunostaining with anti-CatD antibodies; green is immunostaining
1089 with anti-ZP3 antibodies**. (j)** Omission of anti-CatD immunostaining to better visualize the
1090 fragments of DAPI-stained apoptotic oocytes bound to- (**1,3**) and ingested by (**2, 4**) KGN cell as
1091 shown by confocal slicing **(i-k, lower panels). (l)** Western blotting analysis of CatD protein
1092 content during exposure of KGN cells to POS (left) or to apoptotic oocytes (right) with a graph
1093 representing CatD content over time, normalized to CatD content at time 0. **P < 0.001 by
1094 ANOVA test with Bonferroni post hoc analysis. **(m, n, o)** Electron micrographs of control KGN
1095 cells **(m)** and cells challenged with the fragments of apoptotic oocytes (**n**, arrow) or POS (**o**,
1096 arrow). Note the accumulation of lysosomes (ly) in the cytoplasm of cells in **(n)** and **(o). (p)**
1097 Quantification histogram of lysosome content/per nucleus in control KGN cells, and after
1098 exposure to apoptotic oocytes and POS. **(q, r)** Western blotting analysis of sequestosome 1/p62
1099 (p62) protein content during exposure of KGN cells to POS **(q)** and to apoptotic oocytes **(r)** with
1100 a graph representing p62 content over time, normalized to p62 content at time 0; with no
1101 significant differences by ANOVA test with Bonferroni post hoc analysis.
1102
1103
1104 **Supplementary Figure S1** Interaction of human granulosa KGN cell line with apoptotic
1105 substrates,
1106
1107 **(a)** Immunofluorescent pictures of the cultured human granulosa KGN cell line incubated
1108 with the fragments of photoreceptor outer segments (POS), revealed with antibodies against
1109 rhodopsin (Rho) (red). Right panel in **(a)** is the merge of left panel with DIC projection to

Accepted manuscript

1110 better visualize cell shapes. Note the POS in cell periphery (arrow) and close to the nucleus
1111 stained with 4', 6 diamidino-2-phenylindole (DAPI) (arrowhead).
1112 **(b)** Confocal pictures of the cultured granulosa KGN cell line incubated with 1 µm inert
1113 microspheres/beads (green) and stained with anti-autophagy related protein 5 (ATG5) antibody
1114 (red) (left panel). In central and right panels red or green staining were omitted to better
1115 visualize the absence of co-localization.
1116 **(c)** Confocal pictures of the cultured granulosa KGN cell line incubated with 1 µm inert
1117 microspheres/beads (green) and stained with anti-Beclin1 (Bcn1) antibody (red) (leftpanel). In
1118 central and right panels red or green staining were omitted to better visualize the absence of co-
1119 localization.
1120 **(d)** Western blotting (WB) analysis of the content of autophagy related protein 7 (ATG7) in the
1121 lysates of KGN cells during the incubation (hours) with apoptotic oocytes (left panel), or POS
1122 (right panel) with the graphs representing ATG7 content over time, normalized to ATG7 level
1123 at time 0; with no significant differences by ANOVA test with Bonferroni post hoc analysis.
1124 MW: molecular weight markers.
1125 **(e)** Western blotting analysis of the content of microtubule-associated protein 1 light chain 3
1126 (LC3) protein in the lysates of KGN cells after 24 h treatment with 200 nm rapamycin (upper
1127 panel); lower panel – the content of glyceraldehyde-3-phosphate dehydrogenase (GAPDH) in
1128 the same lysates.
1129 **(f)** WB analysis of Cathepsin D (CatD) content in the lysates of human retinal pigment
1130 epithelial hTERT-RPE1 cells challenged with POS. Note the strong band around 50 kDa
1131 corresponding to proCatD.

1132

Accepted manuscript

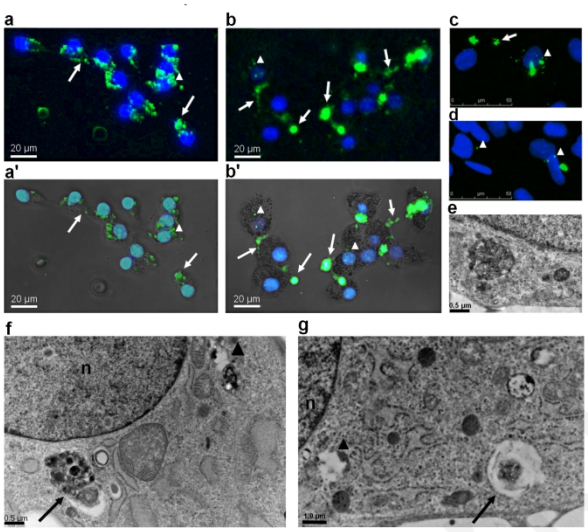

Fig.1

209x297mm (300 x 300 DPI)

Accepted manuscript

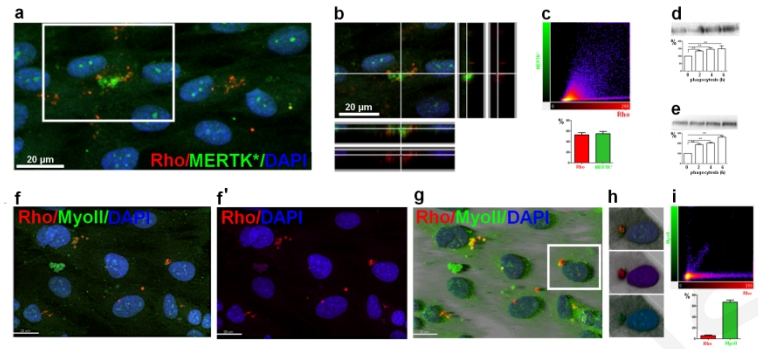

Fig.2

209x297mm (300 x 300 DPI)

Accepted manuscript

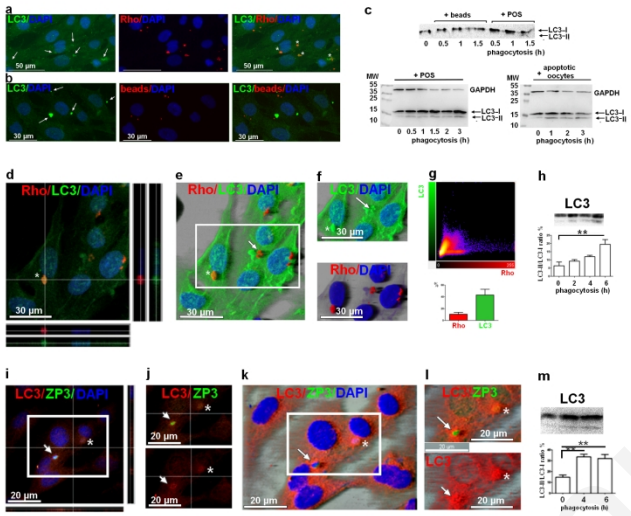

Fig.3

209x297mm (300 x 300 DPI)

Accepted manuscript

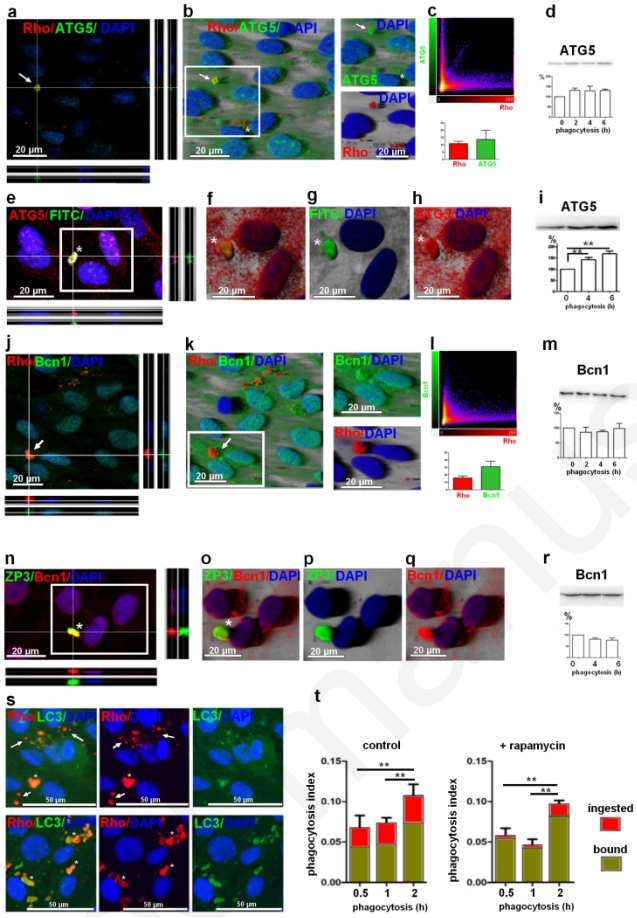

Fig.4

209x297mm (300 x 300 DPI)

Accepted manuscript

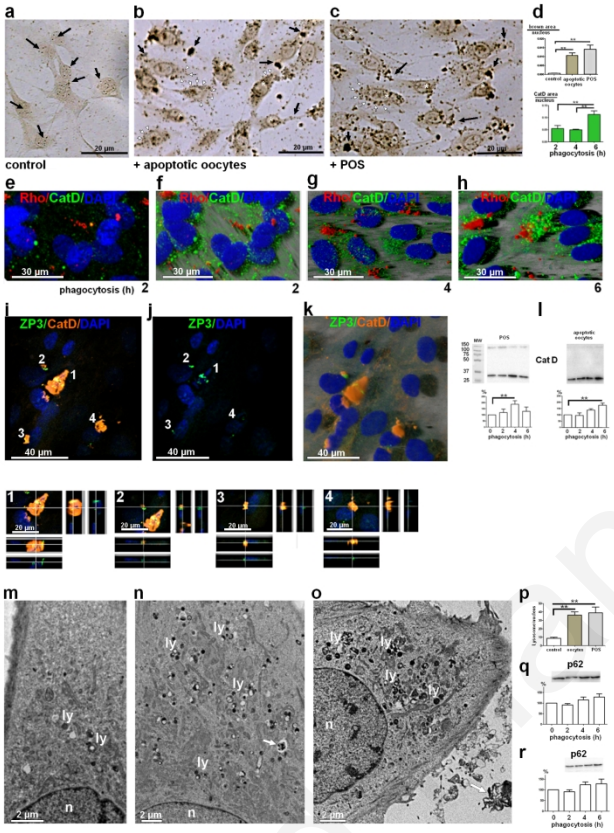

Fig.5

656x928mm (96 x 96 DPI)

Accepted Manuscript

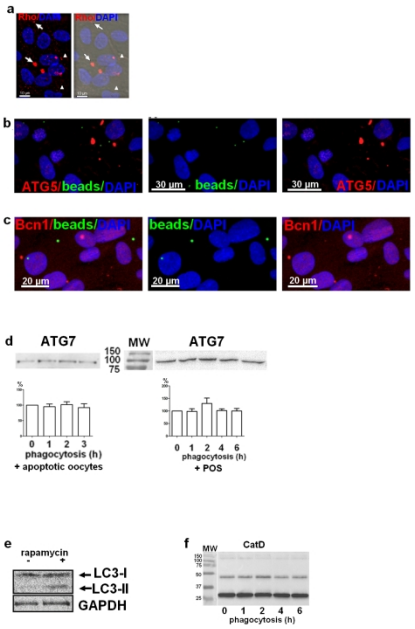

Supplementary Fig.1

209x297mm (300 x 300 DPI)

Accepted manuscript